JGR Space Physics

RESEARCH ARTICLE
10.1029/2024JA033174

Relativistic Electron Flux Decay and Recovery: Relative Roles of EMIC Waves, Chorus Waves, and Electron Injections

Zijin Zhang[1], **Anton Artemyev**[1], **Didier Mourenas**[2,3], **Vassilis Angelopoulos**[1], **Xiao-Jia Zhang**[1,4], **S. Kasahara**[5], **Y. Miyoshi**[6], **A. Matsuoka**[7], **Y. Kasahara**[8], **T. Mitani**[9], **S. Yokota**[10], **T. Hori**[6], **K. Keika**[5], **T. Takashima**[9], **M. Teramoto**[11], **S. Matsuda**[8], and **I. Shinohara**[9]

[1]Department of Earth, Planetary, and Space Sciences, University of California, Los Angeles, CA, USA, [2]CEA, DAM, DIF, Arpajon, France, [3]Laboratoire Matière en Conditions Extrêmes, Université Paris-Saclay, CEA, Bruyères-le-Châtel, France, [4]Department of Physics, University of Texas at Dallas, Richardson, TX, USA, [5]Department of Earth and Planetary Science, School of Science, The University of Tokyo, Tokyo, Japan, [6]Institute for Space Earth Environmental Research, Nagoya University, Nagoya, Japan, [7]Graduate School of Science, Kyoto University, Kyoto, Japan, [8]Graduate School of Natural Science and Technology, Kanazawa University, Kanazawa, Japan, [9]Institute of Space and Astronautical Science, Japan Aerospace Exploration Agency, Sagamihara, Japan, [10]Osaka University, Osaka, Japan, [11]Kyushu Institute of Technology, Faculty of Engineering, Department of Space Systems Engineering, Kitakyushu, Japan

Key Points:

- Multi-satellite observations of EMIC and chorus waves and injections are used to investigate their relative importance in electron dynamics
- We show that chorus-driven acceleration during plasma sheet injections can overcome EMIC-driven losses
- We develop an analytical model of relativistic electron flux variations subject to acceleration and losses

Supporting Information:

Supporting Information may be found in the online version of this article.

Correspondence to:

Z. Zhang,
zijin@ucla.edu

Citation:

Zhang, Z., Artemyev, A., Mourenas, D., Angelopoulos, V., Zhang, X.-J., Kasahara, S., et al. (2024). Relativistic electron flux decay and recovery: Relative roles of EMIC waves, chorus waves, and electron injections. *Journal of Geophysical Research: Space Physics*, *129*, e2024JA033174. https://doi.org/10.1029/2024JA033174

Received 12 AUG 2024
Accepted 3 DEC 2024

Author Contributions:

Conceptualization: Anton Artemyev, Didier Mourenas
Data curation: Zijin Zhang
Formal analysis: Zijin Zhang, Anton Artemyev, Didier Mourenas
Funding acquisition: Anton Artemyev, Vassilis Angelopoulos
Investigation: Zijin Zhang
Methodology: Zijin Zhang, Anton Artemyev, Didier Mourenas
Project administration: Anton Artemyev
Software: Zijin Zhang, Anton Artemyev, Didier Mourenas
Supervision: Anton Artemyev, Vassilis Angelopoulos
Validation: Zijin Zhang
Visualization: Zijin Zhang
Writing – original draft: Zijin Zhang, Anton Artemyev
Writing – review & editing: Didier Mourenas, Vassilis Angelopoulos

Abstract We investigate the dynamics of relativistic electrons in the Earth's outer radiation belt by analyzing the interplay of several key physical processes: electron losses due to pitch angle scattering from electromagnetic ion cyclotron (EMIC) waves and chorus waves, and electron flux increases from chorus wave-driven acceleration of ∼100–300 keV seed electrons injected from the plasma sheet. We examine a weak geomagnetic storm on 17 April 2021, using observations from various spacecraft, including GOES, Van Allen Probes, ERG/ARASE, MMS, ELFIN, and POES. Despite strong EMIC- and chorus wave-driven electron precipitation in the outer radiation belt, trapped 0.1–1.5 MeV electron fluxes actually increased. We use theoretical estimates of electron quasi-linear diffusion rates by chorus and EMIC waves, based on statistics of their wave power distribution, to examine the role of those waves in the observed relativistic electron flux variations. We find that a significant supply of 100–300 keV electrons by plasma sheet injections together with chorus wave-driven acceleration can overcome the rate of chorus and EMIC wave-driven electron losses through pitch angle scattering toward the loss cone, explaining the observed net increase in electron fluxes. Our study emphasizes the importance of simultaneously taking into account resonant wave-particle interactions and modeled local energy gradients of electron phase space density following injections, to accurately forecast the dynamical evolution of trapped electron fluxes.

1. Introduction

There are six important physical processes that affect the dynamics of relativistic (>0.3 MeV) electrons trapped in the Earth's outer radiation belt: (a) electron losses due to pitch angle scattering toward the loss cone via resonant interactions with electromagnetic ion cyclotron (EMIC) waves (Angelopoulos et al., 2023; Millan & Thorne, 2007; Miyoshi et al., 2008; Miyoshi et al., 2008, 2008; Ross et al., 2021; Shprits et al., 2008; Summers & Thorne, 2003; Thorne & Kennel, 1971), (b) electron losses due to pitch angle scattering toward the loss cone via resonant interactions with whistler-mode waves (Horne et al., 2005; Mourenas, Artemyev, Agapitov, & Krasnoselskikh, 2014), (c) electron flux increases due to chorus wave-driven acceleration of $\approx 100-300$ keV ”seed” electrons (Allison & Shprits, 2020; Jaynes et al., 2015; Li et al., 2014; Miyoshi et al., 2003; Mourenas, Artemyev, Agapitov, Krasnoselskikh, & Li, 2014; Thorne et al., 2013) provided by recurrent strong injections (Hua et al., 2022; Mourenas et al., 2023), (d) electron losses due to magnetopause shadowing and outward radial diffusion (Boynton et al., 2016, 2017; Olifer et al., 2018; Shprits, Thorne, Friedel, et al., 2006), (e) electron flux increase due to inward radial diffusion by ULF waves (Ozeke et al., 2014, 2020), and (f) electron flux increase due to direct injections of $\sim 0.5-1.5$ MeV electrons in the outer belt (H.-J. Kim et al., 2021; Tang et al., 2022).

EMIC wave-driven electron precipitation is considered a key contributor to electron losses at energies exceeding the minimum energy for cyclotron resonance with such waves, $E_{\min} \sim 0.5-1$ MeV (Kurita et al., 2018; Nakamura et al., 2022; Summers et al., 2007a; Summers & Thorne, 2003; Usanova et al., 2014), because EMIC wave-driven electron pitch angle scattering rates near the loss cone at such energies are much larger than chorus wave-driven ones (e.g., Glauert & Horne, 2005; Ni et al., 2015; Summers et al., 2007b). And indeed, numerical simulations of the dynamics of the outer radiation belt (Drozdov et al., 2017; Ma et al., 2015; Shprits et al., 2016) and data-model comparisons (Shprits et al., 2017; H. Kim et al., 2021; Drozdov et al., 2022; Adair et al., 2022; Angelopoulos et al., 2023) have demonstrated that EMIC waves can efficiently scatter relativistic electrons and rapidly deplete their fluxes in the outer radiation belt.

But for energies below ultra-relativistic energies (below several MeV) and for typical plasma characteristics, EMIC wave-driven electron scattering mostly affects low pitch angle electrons (equatorial $\alpha_{eq} < 30°$, see Ni et al., 2015; Kersten et al., 2014). It has been suggested that additional high pitch angle($\alpha_{eq} > 30°$) electron scattering by whistler-mode waves can assist EMIC waves in the precipitation of the near-equatorial (trapped) electron population (Mourenas et al., 2016; X.-J. Zhang et al., 2017; Drozdov et al., 2020). Indeed, it has been shown that a combination of electron scattering by EMIC and whistler-mode waves at the same L-shell (even if at different longitudes) can result in a very effective electron flux depletion (Mourenas et al., 2016; H. Kim et al., 2021; Drozdov et al., 2022).

In addition, there is a competition between electron acceleration by chorus waves (produced by anisotropic electrons that are directly adiabatically heated during injections, see, e.g. Sorathia et al., 2018) and electron precipitation by EMIC and chorus waves, and this dynamic competition ultimately results in the observed radiation belt electron flux time-series, and also its energy spectrum, in response to multiple injections. In particular, recent work has shown that in the presence of sustained injections and both energy diffusion by chorus waves and pitch angle diffusion by chorus and/or EMIC waves, the normalized electron flux energy spectrum $J(E)$ at $\sim 0.1-2$ MeV should dynamically tend toward a steady-state normalized energy spectrum $J_{UL}(E)$, which represents an attractor for the system dynamics and corresponds to a balance, at each energy, between electron flux increase and electron flux loss, fine-tuned by the electron phase space density (PSD) energy gradient (Hua et al., 2022; Mourenas, Artemyev, et al., 2022a; Mourenas et al., 2023; Summers & Stone, 2022). This suggests that a net flux decrease (increase) should occur when $J(E)$ decreases with energy less (more) rapidly than the steady-state attractor energy spectrum $J_{UL}(E)$, corresponding to a sufficiently mild (steep) PSD decrease with energy (Mourenas, Artemyev, et al., 2022a; Mourenas et al., 2023).

Although injections of anisotropic $\sim 1-100$ keV "source" ions and electrons from the plasma sheet can simultaneously drive EMIC (Jun et al., 2019, 2021) and chorus waves (Miyoshi et al., 2013; Jaynes et al., 2015; Tao et al., 2011; Fu et al., 2014; X. Zhang et al., 2018), these particle injections do not fully determine the associated wave power (which also depends on Landau damping and cold plasma density as well as the spatio-temporal extent and intensity of injections), nor do they directly control the impact of these waves on electrons (since this impact also depends on cold plasma density, wave power, and Landau damping during wave propagation, with/without wave ducting). Accordingly, EMIC and chorus wave-driven electron scattering can be examined separately from injections, traditionally on the basis of event-based or statistical wave measurements.

However, one cannot prove that more injections preferentially cause a flux increase at relativistic energies (through an increase of $\sim 100-300$ keV seed electron flux accompanied by chorus wave-driven electron acceleration to higher energies) as opposed to a flux decrease (through more precipitation by EMIC and/or whistler-mode waves generated by injections). In this paper, we will show qualitatively that there is an association of higher injection rate with higher rate of chorus wave-driven electron energy diffusion and flux increase that helps overcome the rate of EMIC wave-driven pitch angle scattering and flux decrease. This event is illustrative, and more cases like that (or a statistical analysis) may help prove or refute this conjecture in the future.

In this study, we investigate a fortuitous conjunction between equatorial and low-altitude satellites, which enables direct observations of electron loss due to scattering by EMIC and whistler-mode waves, electron acceleration by whistler-mode waves, and plasma sheet injections. This allows us to examine the first three mechanisms listed above near $L \sim 5$ in the outer radiation belt. During the investigated period, direct injections of 0.5–1.5 MeV electrons at $L \sim 5-5.5$ are assumed to be absent based on the rarity of >600 keV injections at $L \leq 5.5$ in statistical observations from the Van Allen probes (Tang et al., 2022), and no significant dropout should have occurred due to weakly negative IMF B_z and low solar wind dynamic pressure $Pdyn$ (see details below). Combining spacecraft observations during this event with theoretical estimates of electron scattering rates, we show that even long-lasting ($\sim$4 hours) electron losses driven by EMIC waves cannot deplete $\sim 0.1-1.5$ MeV electron fluxes in the outer radiation belt if plasma sheet electron injections are sufficiently strong. Resupply of relativistic electron fluxes can occur due to chorus wave-driven acceleration of freshly injected $\sim 100-300$ keV seed electrons.

The structure of this paper includes Section 2 with the general description of spacecraft instruments and the event overview, Section 3 describing near-equatorial observations of plasma sheet injections during the event, Section 4 describing low-altitude observations of EMIC wave-driven electron precipitation, Section 5 assessing the relative importance of chorus waves in compensating for the EMIC wave-driven electron precipitation losses, and Section 6 summarizing the obtained results.

2. Spacecraft and Data Set

In this study we use low altitude measurements of ELFIN A and B CubeSats (Angelopoulos, Tsai, et al., 2020) that provide energy (16 channels within [50, 6,000] keV) and pitch angle (8 channels within $[0, 180°]$) resolved electron flux measurements. We mainly use electron fluxes averaged within the local loss cone (precipitating fluxes, j_{prec}) and outside the local loss cone (trapped fluxes, j_{trap}), and the precipitating-to-trapped flux ratio, j_{prec}/j_{trap}. ELFIN measurements are used to reveal the energy range and L-shell (determined from magnetic field models) localization of EMIC wave-driven electron precipitation, distinguished by a typical peak of j_{prec}/j_{trap} at relativistic energies (see examples of such EMIC wave-driven precipitation events in Grach et al., 2022b; X. An et al., 2022; Angelopoulos et al., 2023). To confirm our interpretation that electron precipitation bursts are associated with EMIC waves, we use POES/NOAA measurements of energetic proton precipitation (Evans & Greer, 2004) within the same MLT sector. Such proton precipitation bursts are generally a good indication of the equatorial EMIC wave source region (see discussion in A. Yahnin & Yahnina, 2007; A. G. Yahnin et al., 2017; Capannolo et al., 2023).

The equatorial measurements of energetic electron and ion fluxes are obtained from the fleet of spacecraft: GOES-16 and 17 provide [70,1000] keV ion and electron fluxes (Boudouridis et al., 2020; Dichter et al., 2015), Magnetospheric Multiscale (MMS) mission (Burch et al., 2016) provide [50, 500] keV ion and electron fluxes (Blake et al., 2016; Mauk et al., 2016), Exploration of energization and Radiation in Geospace (ERG/Arase) spacecraft (Miyoshi, Shinohara, Takashima, et al., 2018) provide [20, 120] keV ion fluxes (Yokota et al., 2017) and [10, 2,000] keV electron fluxes (S. Kasahara, Yokota, Mitani, et al., 2018; Mitani, Takashima, et al., 2018). We also use ERG wave instrument (Y. Kasahara, Kasaba, et al., 2018; Matsuda et al., 2018) providing magnetic field spectrum in the whistler mode frequency range, and GOES(Singer et al., 1996), MMS(Russell et al., 2016), and ERG (Matsuoka, Teramoto, Nomura, et al., 2018) magnetometers for DC magnetic field measurements.

Figure 1 shows the orbits of all spacecraft that provided the data analyzed in this study. The event on 17 April 2021 was selected due to the presence of a series of strong injections and significant whistler-mode and EMIC wave activity, at a time when various spacecraft measurements were simultaneously available, providing a comprehensive view of the processes affecting relativistic electron fluxes. In addition, this event occurred during the main and early recovery phase of a moderate storm, when Dst varied weakly, suggesting a weak adiabatic Dst effect on electron fluxes at $L \simeq 5.5$ (H.-J. Kim & Chan, 1997). The IMF B_z and the dynamic pressure of the solar wind $Pdyn$ indicate that the magnetopause remained at $L > 9$, suggesting an absence of the magnetopause shadowing loss of electrons at $L < 6$ during that period (ALbert et al., 2018; Shue et al., 1997), while the electron radial diffusion by ULF waves (Ozeke et al., 2014) should remain relatively moderate for an average $Kp \sim 4$ at $1-11$ UT (a more detailed discussion of these two physical processes is provided in Section 5.3). Accordingly, the selected period on the morning of 17 April 2021 looks favorable for analyzing the interplay between EMIC wave-driven electron loss, chorus wave-driven electron loss, and chorus wave-driven electron acceleration in the heart of the outer radiation belt.

The sequence of events on 17 April 2017 is as follows.

- At $\sim$01:15 UT: ERG observed strong electron injections that were probably responsible for whistler-mode wave generation (the onset of chorus waves coincides with this injection).
- At 01:30–02:30 UT: GOES-16&17 observed strong ion injections that arrived at ELFIN's MLT (∼16.5) around 02:30-03:00 UT (based on ion azimuthal drift estimates) and should have driven EMIC wave generation.

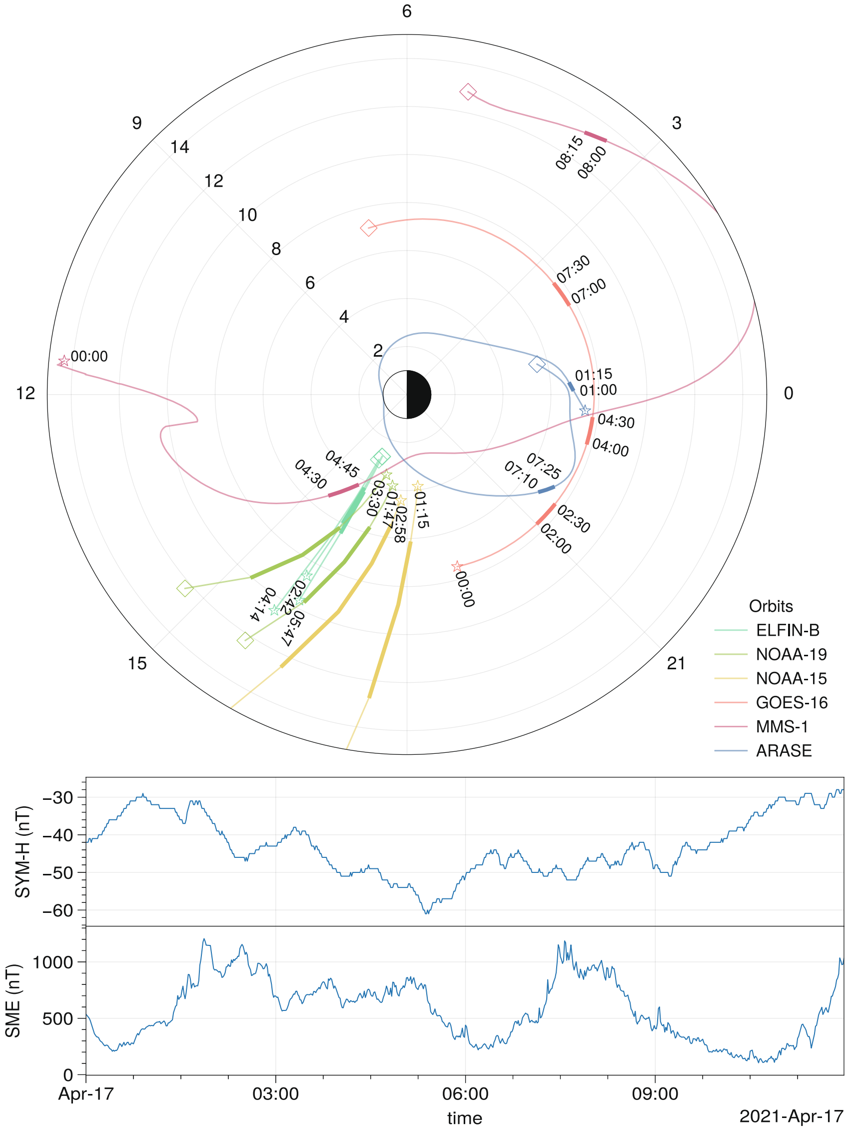

Figure 1. (top) An overview of the mission orbits recorded on 17 April 2021, from 00:00 to 12:00 UTC. The orbits of the various missions are projected onto the MLT and *L*-shell plane, using Tsyganenko 2001 model (Tsyganenko, 2002a, 2002b) for active conditions. Distinct colors differentiate between missions, with stars marking the commencement of orbits, squares indicating their termination points, and temporal annotations highlighting the periods of interest. ELFIN-B's trajectory is displayed during three time intervals: 02:42–02:46, 04:14–04:18, and 05:47–05:51 UT. NOAA-19's trajectory is plotted for 01:47–01:52 and 03:30–03:36 UT, while NOAA-15's is displayed at 01:15–01:20 and 02:58–03:03 UT. The trajectories of GOES, MMS, and Arase span the entire 12-hr interval from 00:00 to 12:00 UT (bottom) Sym-H and SME indices during this event.

- At 02:40–06:00 UT: ELFIN observed continuous precipitation of relativistic electrons at MLT ~16; NOAA/POES observations of ion isotropic boundary at the same latitudes as ELFIN observations suggest relativistic electron precipitation are located right at the inner edge of the ion plasma sheet. To support such precipitation by EMIC waves, whistler-mode waves recorded by ERG (at MLT ~ 20) should continuously scatter relativistic electrons from higher equatorial pitch angles into the pitch angle range resonating with EMIC waves.
- At 07:10–07:30 UT: ERG and GOES-16&17 observed a strong electron injection: dispersionless on ERG (MLT ~ 20) and dispersive on GOES-17 (MLT ~ 4). This injection appears to restore electron fluxes and largely compensate for losses from EMIC wave-driven scattering, at least at $E \leq 1.5$ MeV.

- Between ~07:00–10:00 UT: ERG observed significant increases of >0.5 MeV fluxes at $L \sim 5.7$. Our study is specifically focused on the mechanisms potentially explaining this local acceleration preceded by EMIC-driven losses and plasma sheet injections.

Some elements of this scenario are also observed by the MMS spacecraft.

3. Plasma Sheet Injections

In this section, we describe plasma sheet injections observed by near-equatorial GOES-16&17, MMS, and ERG spacecraft.

Figure 2 shows GOES-16&17 ion and electron fluxes for the first 12 hours of 17 April 2021: GOES spacecraft started at pre-midnight local time (MLT ~ 19) and traveled along geostationary orbit until it reached MLT ~ 7 at 12:00 UT. At 1:30 UT, both GOES spacecraft detected strong ion injections (almost dispersionless at GOES-16 around MLT ~ 20, and quite dispersive at GOES-17 around MLT ~ 16). Between 01:30 and 07:00 UT, the GOES spacecraft detected a series of ion and electron injections. Finally, at 07:10-07:30 UT GOES spacecraft detected a very strong substorm injection: a dipolarization of the magnetic field, with B_x, B_y magnitude decrease and B_z increase (both spacecraft are at the night side, MLT ~ 22−3, and detect typical plasma sheet substorm dynamics) and the increase of electron and ion fluxes, by more than one order of magnitude. The electron flux increase is almost dispersionless at GOES-16 and slightly dispersive at GOES-17 (located more dawnward). Ion injections are quite dispersive on both GOES spacecraft, as ions have to drift around the Earth from dusk to dawn.

Figure 3 shows the ERG observations of the ≤100 keV ion and electron flux. The first two panels show an increase in electron and proton fluxes at approximately 01:00 UT and 07:10 UT. The first strong injection observed at ~01:00 UT, around midnight (MLT ~ 0) was associated with an onset of whistler-mode wave activity (discussed below). Then ERG moved to the post-midnight sector and observed a series of electron injections (between 01:30 and 03:00 UT), also detected by GOES-16&17 (see Figure 2). Moving past its perigee, ERG reached the pre-midnight sector (MLT ~ 21) after 06:00 UT, and then detected a very strong substorm injection at 07:10 UT (also recorded by GOES-16&17). At 07:00 UT ERG was at middle latitudes (MLAT ~ 25°) and, thus, ERG observed a very clear electron flux depletion during the substorm growth phase (when the spacecraft effectively moves away from the equator due to magnetic field line stretching; see Artemyev et al. (2016); Angelopoulos, Artemyev, et al. (2020)). A similar, but less evident, electron flux depletion is seen at the equatorial GOES-16 (see Figure 2). The substorm onset is associated with electron flux increase and magnetic field dipolarization (B_z increase), which is weaker at middle latitudes covered by the ERG than at the equatorial GOES-16 data.

Figure 4 shows the MMS observations of the <500 keV ion and electron fluxes. The spacecraft were in the magnetosheath at the beginning of the time interval, and crossed the magnetopause, entering the magnetosphere, around 02:30 UT. Around 04:45 UT MMS were within the region where ELFIN observed EMIC wave-driven precipitation (see below), and there MMS detected a spatially localized decrease of >300 keV electron fluxes. This decrease may be interpreted as the result of energetic electron loss driven by EMIC waves (Angelopoulos et al., 2023; Denton et al., 2019; Drozdov et al., 2020; Hendry et al., 2019). Around 07:30-08:00 UT MMS observed dipolarization (B_z variations) and electron and ion flux increases in the near-Earth plasma sheet (at $L > 9$). This is likely the same substorm injection that ERG and GOES detected at ~07:30 UT (see Figures 2 and 3).

Overall GOES, ERG, and MMS observations (Figures 2–4) show two series of strong injections. The first series took place within 01:00-02:00 UT; it transported energetic electrons and ions that drove whistler-mode wave and EMIC wave generation: ERG recorded an appearance of intense whistler-mode waves at ~01:00 UT, and intense EMIC waves have been indirectly detected through ELFIN observations of strong relativistic electron precipitation (see Section 4 and Figure 5 below). The second series of injections occurred at 07:00-08:00 UT, bringing in energetic electrons that filled back the depleted radiation belt population.

4. EMIC Wave Driven Precipitation

Figure 5 shows the precipitating-to-trapped flux ratio j_{prec}/j_{trap} during four ELFIN orbits, with the clear signatures of EMIC wave-driven precipitation (a full information about ELFIN measurements for the entire interval, 00:00-12:00 UT, can be found in Supporting Information S1). Within $L \in [5,6]$ there is a peak of precipitating-to-trapped flux ratio above 300 keV. This peak moves from $L \sim 6$ around 02:45 UT to $L \sim 5$ at 05:15 UT.

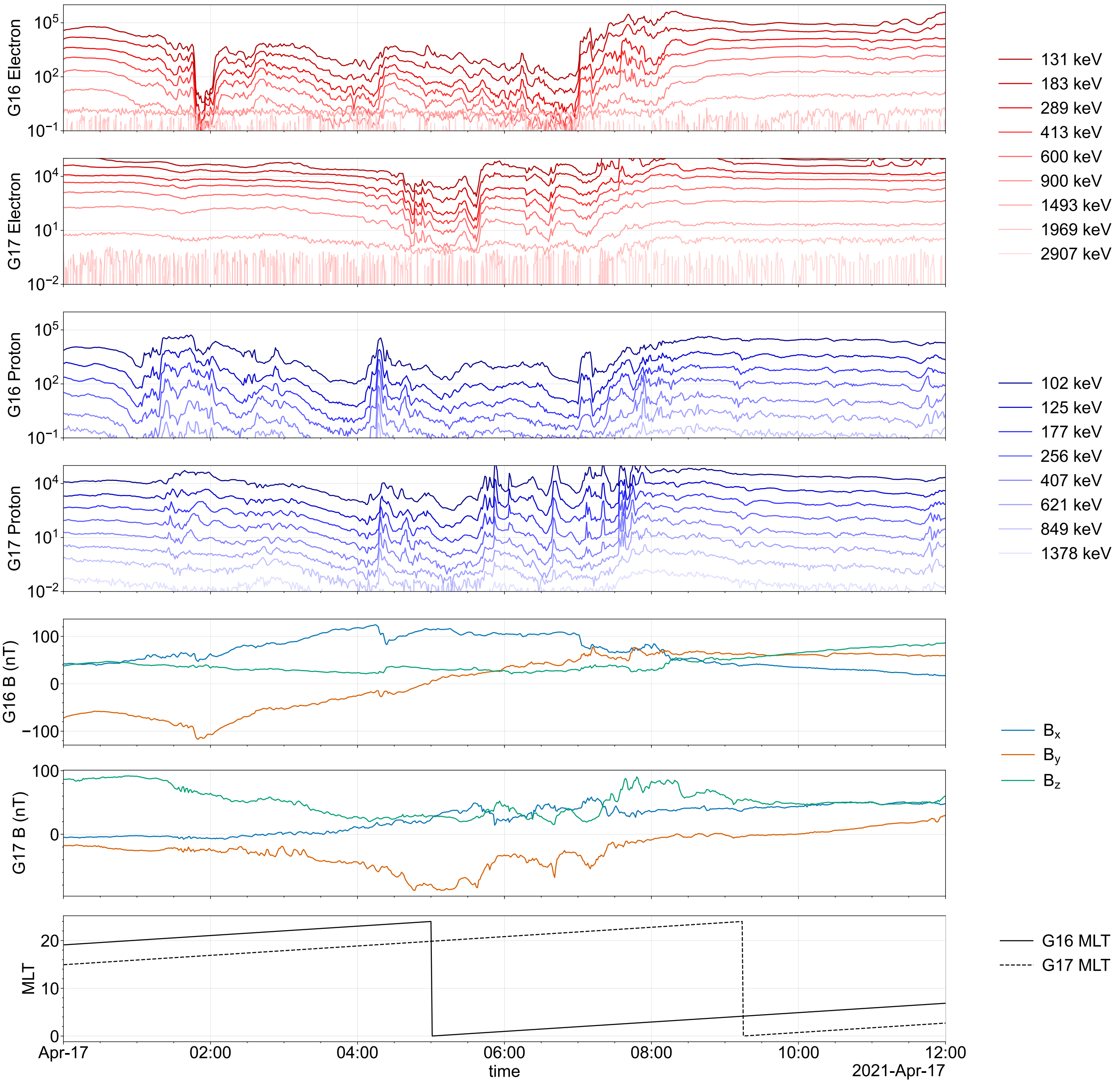

Figure 2. GOES-R electron and proton flux observations (70 keV to ~1 MeV) from two geostationary operational satellites. Ion injections are seen from 2 UT (right when ELFIN starts observing EMIC wave-driven precipitation) to 8 UT. A series of strong electron injections are observed around 07:10–07:30 UT at MLT $\sim 2 - 3$ after drifting from midnight.

Only EMIC wave-driven precipitation may have a low energy cut-off point of scattering fluxes around ~500 keV, which is a typical minimum resonance energy for EMIC waves (see the identification of other EMIC wave-driven precipitation events with similar precipitating-to-trapped ratios in X. An et al., 2022; Grach et al., 2022b; Capannolo et al., 2023; Angelopoulos et al., 2023).

Note that the efficient precipitation (large j_{prec}/j_{trap}) observed at $L > 6.5$ is likely due to a combination of whistler-mode wave-driven precipitation (see, e.g., X. Shi et al., 2022; Tsai et al., 2022) and precipitation due to the curvature scattering (e.g., Wilkins et al., 2023), while precipitation of <300keV electrons at $L < 5$ is driven by whistler-mode wave scattering (see similar examples of quasi-periodical precipitation on the dusk flank in Artemyev et al., 2021; X.-J. Zhang et al., 2023).

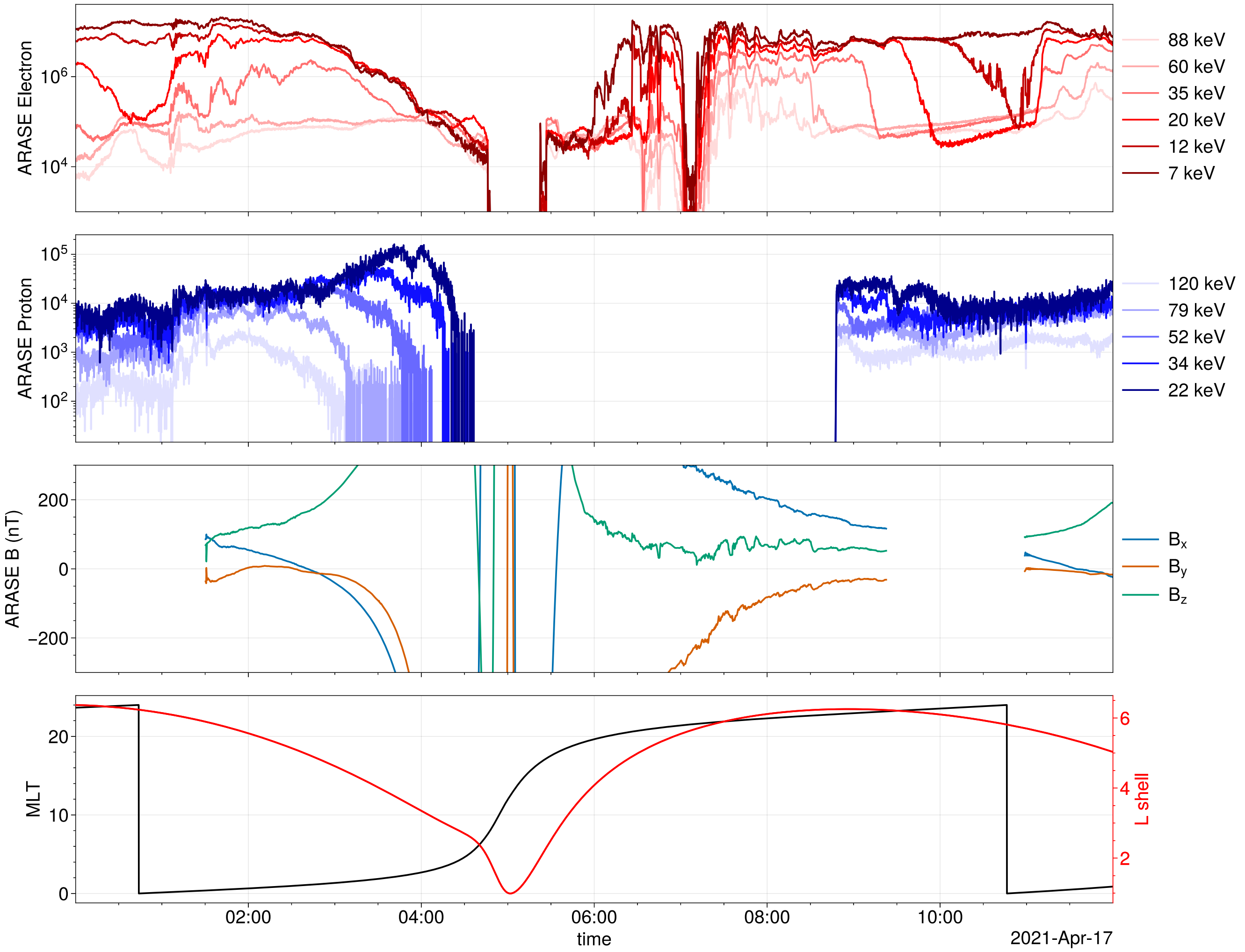

Figure 3. ERG (Arase) electron and proton flux observations (~10 keV to ~120 keV). Strong electron injections are visible at the beginning of EMIC wave-driven electron precipitation and at the end of the time interval.

Therefore, Figure 5 demonstrates that during at least 3 hours, ELFIN observed continuous EMIC wave-driven losses of relativistic electrons. Note that this period may be $\sim$1.5 hour longer, as the nearest ELFIN orbits without signature of EMIC wave-driven precipitation are at 08:50UT (see the Supporting Information S1). As j_{prec}/j_{trap} for ~0.3–1 MeV electrons reaches one, the strong diffusion regime (see Kennel, 1969), one may expect a significant depletion of equatorial electron flux in this energy range, at least at low pitch angles (e.g., Drozdov et al., 2020; Usanova et al., 2014).

Although ELFIN energetic particle detectors can measure >50 keV ions (Angelopoulos, Tsai, et al., 2020), these measurements were not available during our event. Thus, we use POES/NOAA ion measurements around the same MLT and UT to confirm the presence of EMIC waves (<100 keV ion precipitation is often used as an indication of the presence of EMIC waves, see, e.g., Carson et al., 2013; Miyoshi et al., 2008; H. Kim et al., 2021; A. G. Yahnin et al., 2016). Figure 6 shows four POES/NOAA orbits with ion precipitating and trapped fluxes for two energy ranges. The L-shell range >5 is characterised by isotropic precipitation $\left(j_{prec}/j_{trap} \sim 1\right)$, and such precipitation should be attributed to magnetic field curvature ion scattering (e.g., Dubyagin et al., 2002; Sergeev et al., 2011). Therefore, the inner edge of the ion plasma sheet reached $L \sim 5.5$ during this event. Earthward from the isotropic precipitation, between $L \sim 4.5$ and 5.5, POES/NOAA shows bursty precipitating ion fluxes with a magnitude lower than trapped fluxes. Such precipitation bursts are likely due to ion scattering by EMIC waves. Therefore, POES/NOAA observations confirm the presence of EMIC waves within the same MLT sector as

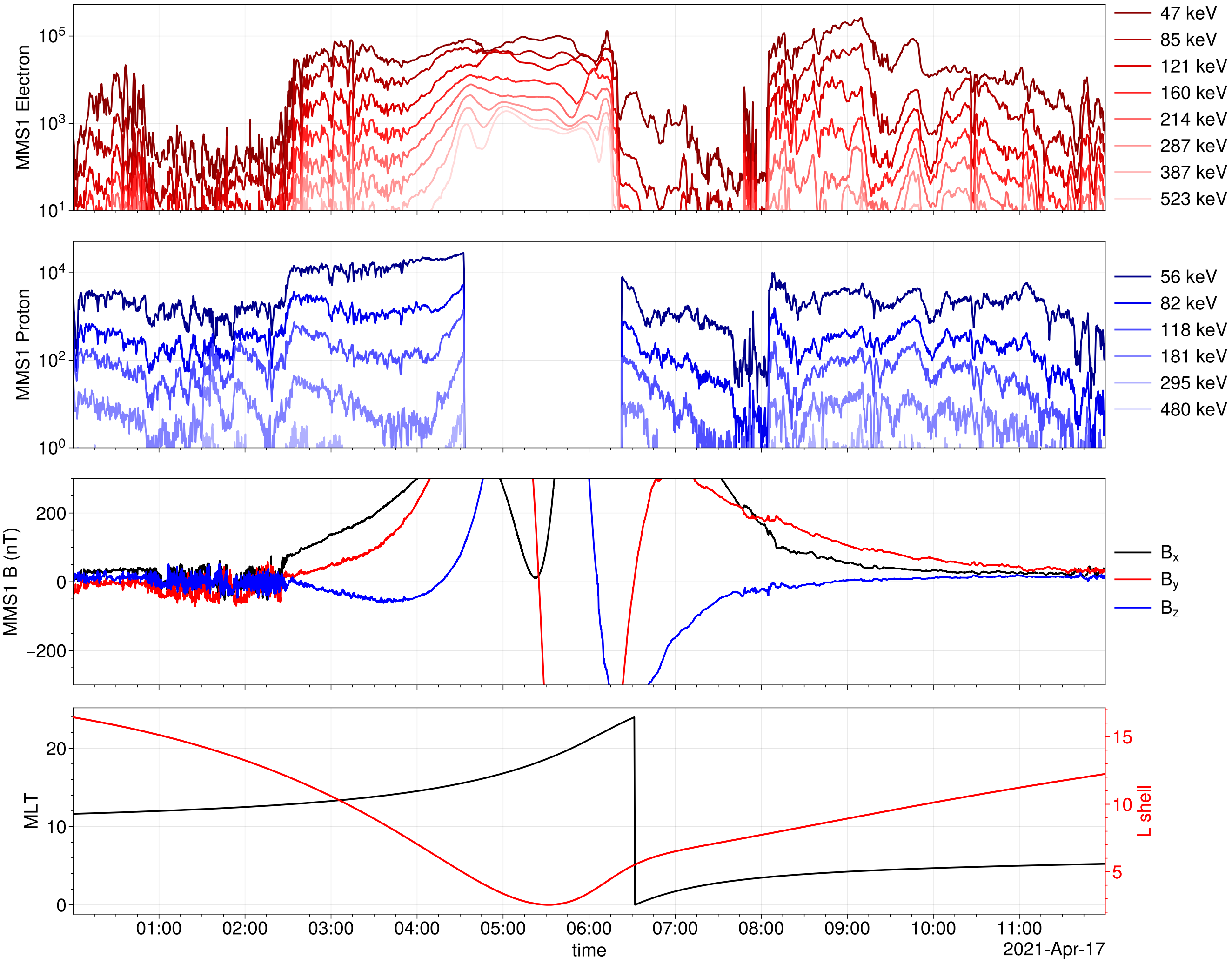

Figure 4. MMS electron and proton flux observations (~50 keV to ~500 keV). A localized decrease of electron fluxes is notable around the time of ELFIN observations of EMIC wave-driven electron precipitation (around 04:30 UT, at MLT ~16).

ELFIN observations and additionally suggest that the inner edge of the ion plasma sheet (actually the region of penetration of plasma sheet injections) reached $L \sim 5.5$.

5. Wave-Driven Electron Diffusion and Flux Variations

In the absence of dropouts related to magnetopause shadowing (Boynton et al., 2016; Matsumura et al., 2011; Shprits, Thorne, Horne, & Summers, 2006; Turner, Shprits, et al., 2012), five main processes can modify the flux of trapped electrons at $L = 5 - 7$: EMIC wave-driven electron precipitation into the atmosphere (Thorne & Kennel, 1971; Albert, 2003; Summers & Thorne, 2003; Sandanger et al., 2007; Miyoshi et al., 2008; Usanova et al., 2014; Blum et al., 2015; Gao et al., 2015; X. J. Zhang et al., 2021), chorus wave-driven electron precipitation and/or acceleration (Horne et al., 2005; Ma et al., 2020; Thorne et al., 2013), and injections from the plasma sheet and/or ULF wave-driven electron radial diffusion (Gabrielse et al., 2014; Ozeke et al., 2014; Runov et al., 2015; Turner, Shprits, et al., 2012). We examine in the following the effects of these different processes, alone or in combination, on the trapped electron flux.

Figure 7 provides a schematic diagram of these different physical processes and of their possible consequences on trapped electron fluxes, indicating the direct effects of injections from the plasma sheet in generating EMIC and chorus waves in different spatial regions (top), and the two possible final outcomes, for trapped electron fluxes $J(E,t)$, of the interplay between injections and wave-driven electron diffusion by EMIC and chorus waves

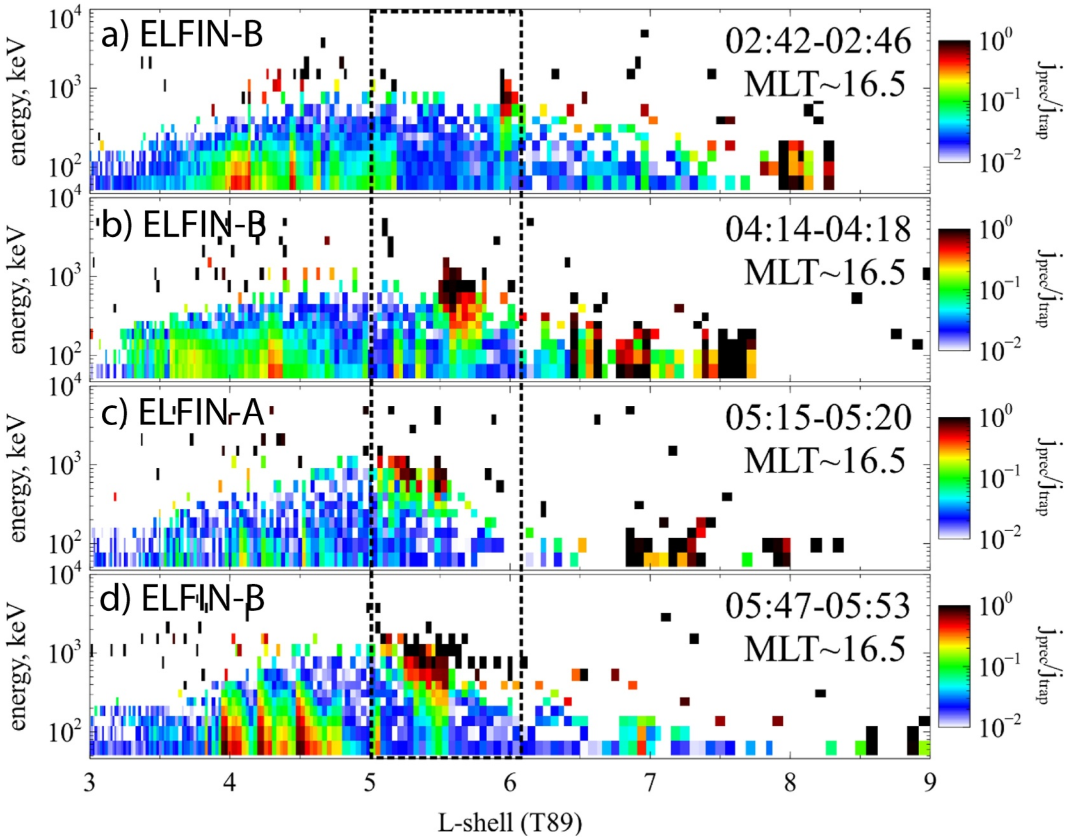

Figure 5. Two ELFIN CubeSats observations of EMIC wave-driven electron precipitation, where the precipitating flux reaches the trapped flux in high-energy channels, over an interval exceeding 3 hours, from 02:42 to 05:53 UT. The locations are projected to the equatorial *L*-Shell and MLT, using the Tsyganenko (1989) magnetic field model. Panels (a), (b), and (d) show data from ELFIN-B, while panel (c) features observations from ELFIN-A.

(bottom), that is, either a flux decrease (bottom left) or a flux increase (bottom right), depending on the initial energy gradient of $J(E,t_0)/J(E_0,t_0) = J_{in}(E,t_0)/J_{in}(E_0,t_0)$ (or of the electron phase space density) compared with the energy gradient of the steady-state attractor, $J_{ul}(E)$ which depends on the ratio of total electron pitch-angle diffusion rates and energy diffusion rates (Hua et al., 2022; Mourenas, Artemyev, et al., 2022b; Mourenas et al., 2023). Below, the different physical mechanisms related to wave-driven electron scattering will first be discussed separately, before examining their combined effects on trapped electron fluxes.

5.1. Role of EMIC Waves Alone

During disturbed periods, intense EMIC waves are often present in the 10–18 MLT noon-dusk sector in a plasmaspheric high-density region (often at the edge of the plasmasphere or inside a plasmaspheric plume), corresponding to a high plasma frequency to gyrofrequency ratio $f_{pe}/f_{ce} > 15$ (Kersten et al., 2014; Meredith et al., 2014; Ross et al., 2021). Such left-hand polarized, quasi-parallel EMIC waves are generated by substorm ion injections in the dusk sector (Cornwall et al., 1970; Horne & Thorne, 1993; Kozyra et al., 1997; L. Chen et al., 2010; H. Chen et al., 2020) and by solar wind pressure enhancements around noon (Olson & Lee, 1983; Usanova et al., 2010; H. Chen et al., 2020; Ross et al., 2021).

When EMIC waves in the H-band have a sufficiently high frequency $f \geq 0.4\, f_{cH}$, with f_{cH} the proton gyrofrequency, they can reach cyclotron resonance with high energy electrons above $\sim 1-2$ MeV near the loss cone and lead to their fast precipitation into the atmosphere via quasi-linear diffusion (Albert, 2003; Meredith et al., 2003; Summers & Thorne, 2003) or through non-linear interactions (Albert & Bortnik, 2009; Grach et al., 2022a; Kubota et al., 2015; Kubota & Omura, 2017). Even in the case of intense EMIC wave-packets, when such packets remain relatively short and are separated by random frequency and phase jumps as in various observations

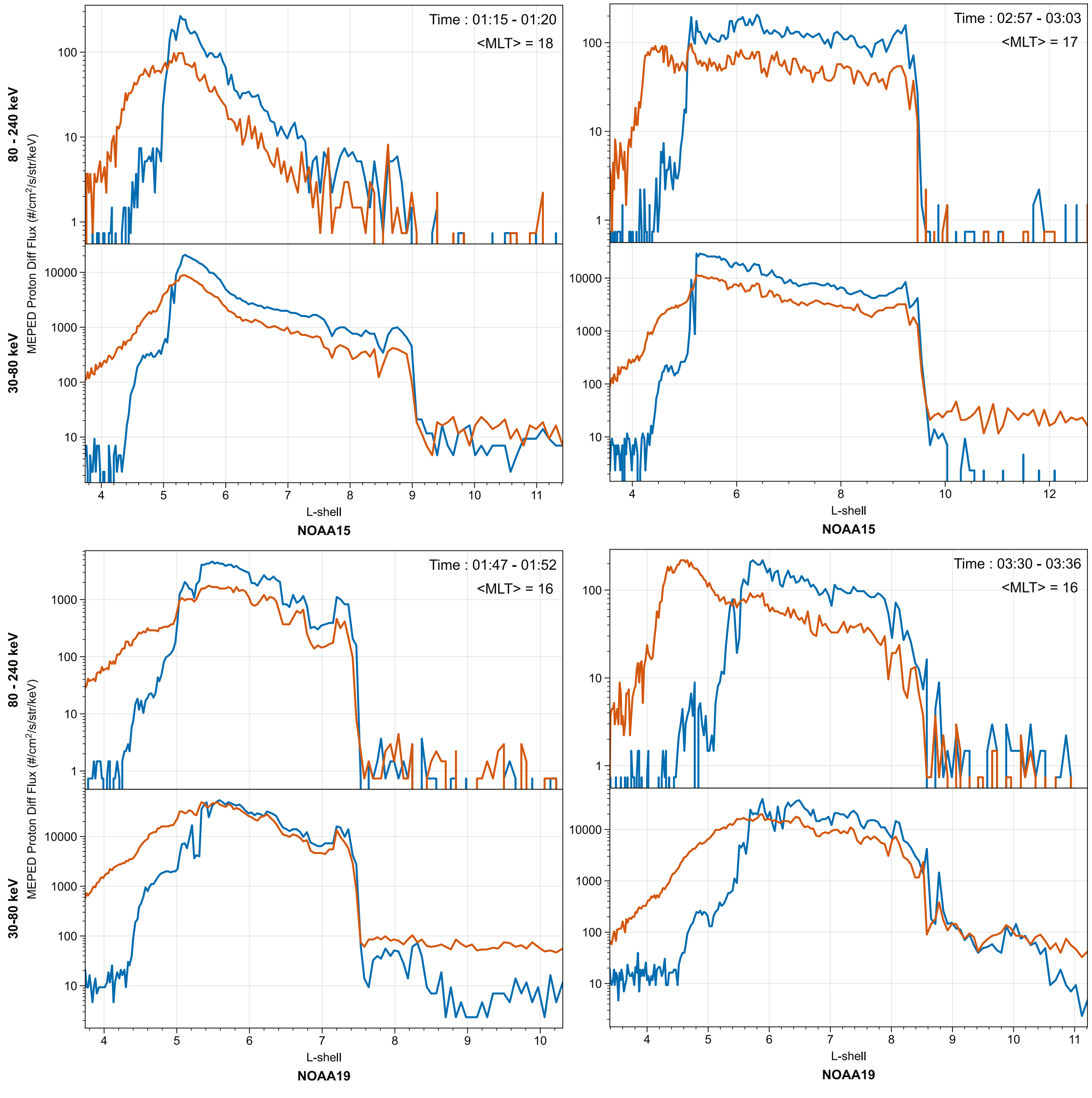

Figure 6. POES observations of proton precipitating (blue) and trapped (orange) fluxes. Four orbits are shown (for each orbit two energy ranges).

(Usanova et al., 2010; X. An et al., 2022), electron transport should still be amenable to a quasi-linear diffusive treatment (X. J. Zhang, Agapitov, et al., 2020; Artemyev et al., 2022). However, the most intense H-band EMIC waves usually reach not-too-high frequencies and, therefore, cannot reach cyclotron resonance with electrons of energy $E < 3$ MeV up to high equatorial pitch angles $\alpha > 60°$ (Kersten et al., 2014; Ross et al., 2021; Summers & Thorne, 2003), preventing them from leading, alone, to a significant decrease of the omnidirection trapped electron flux mainly present at $\alpha > 60°$ (Mourenas et al., 2016).

The maximum equatorial pitch angle $\alpha_{\max}$(EMIC) of electrons of energy E (in MeV) reaching cyclotron resonance with H-band EMIC waves is given by (Mourenas et al., 2016; Summers & Thorne, 2003):

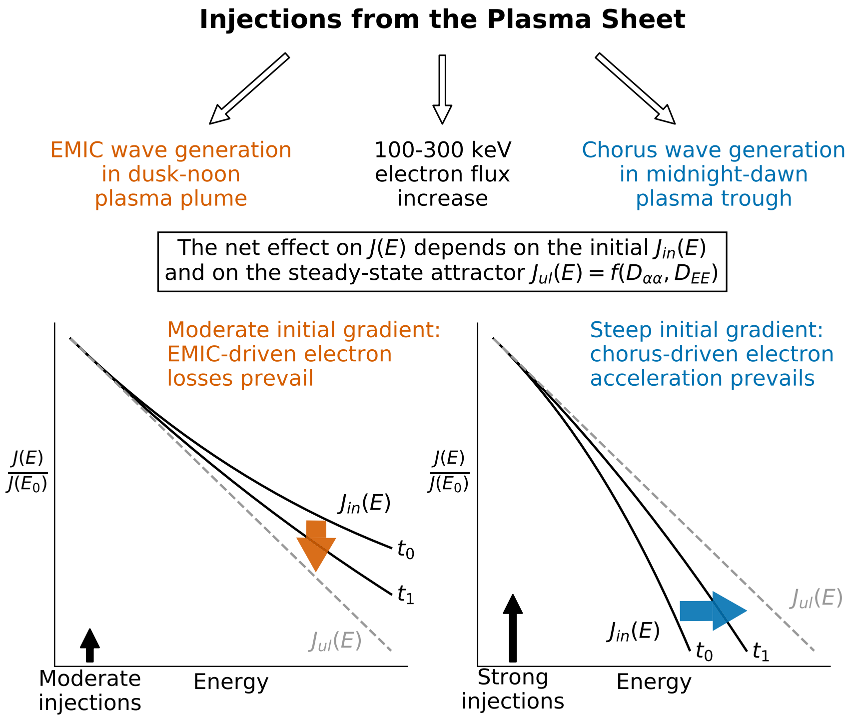

Figure 7. Schematic diagram of the different physical processes and of their possible consequences on trapped electron fluxes (top) Direct effects of (ion and electron) injections from the plasma sheet in generating EMIC and chorus waves in different spatial regions (bottom) The two possible effects of the interplay between injections and wave-driven electron diffusion by EMIC and chorus waves on trapped electron fluxes $J(E)$: a flux decrease from t_0 to t_1 when low-energy injections are too weak to provide a sufficiently steep initial (at t_0) negative energy gradient of electron phase space density, such that $\partial(J_{in}(E,t_0)/J_{in}(E_0,t_0))/\partial E > \partial(J_{ul}(E,t_0)/\ J_{ul}(E_0,t_0))/\partial E$ (where $J_{ul}(E)$ denotes the steady-state attractor flux shape, see Hua et al. (2022); Mourenas et al. (2023)), leading to a prevalence of EMIC (and chorus) wave driven electron losses over chorus-driven electron energization (bottom left), or a flux increase from t_0 to t_1 when strong low-energy electron injections provide a steep initial negative energy gradient of electron phase space density, such that $\partial(J_{in}(E,t_0)/J_{in}(E_0,t_0))/\partial E < \partial(J_{ul}(E,t_0)/J_{ul}(E_0,t_0))/\partial E$, leading to a prevalence of chorus-driven electron energization over EMIC and chorus wave driven losses (bottom right).

$$\cos\alpha_{\max}(\mathrm{EMIC}) \simeq \frac{\Omega_{ce}^2}{2\omega_{\mathrm{EMIC}}\Omega_{pe}} \times \sqrt{\frac{(1-\omega_{\mathrm{EMIC}}/\Omega_{cp})\,(m_e/m_p)}{(E^2+E)}} \tag{1}$$

for a quasi-parallel H-band EMIC wave frequency to proton gyrofrequency ratio $\omega_{\mathrm{EMIC}}/\Omega_{cp}$ at the equator in a plasma usually composed of protons with only a small fraction (<5%) of helium ions during observations of such waves (Kersten et al., 2014). Figure 8 shows $\alpha_{\max}(\mathrm{EMIC})$ as a function of energy and $\omega_{\mathrm{EMIC}}/\Omega_{\mathrm{cp}}$ at $L = 5$, based on an empirical model of plasma density inside the plasmasphere (Sheeley et al., 2001). Low energy (<1 MeV) electron precipitation by H-band EMIC waves can be obtained only for $\omega_{\mathrm{EMIC}}/\Omega_{\mathrm{cp}} > 0.65-0.7$.

An analytical estimate (validated by comparisons with numerical simulations) of the bounce-averaged pitch angle diffusion rate $D_{\alpha\alpha}$ of relativistic (>1 MeV) electrons by H-band EMIC waves near the loss cone has been provided in Equation 1 from (Mourenas et al., 2016). Multiplying this estimate of $D_{\alpha\alpha}$ by a factor $(1+2E)/\left(4E^2+4E\right)^{1/2}$ (and multiplying its inner variable G_0 by the square of the same factor) allows us to extend the validity of this expression of $D_{\alpha\alpha}$ to lower energy electrons (Angelopoulos et al., 2023; Su et al., 2012).

Based on quasi-linear theory in the limit of near-equilibrium of the electron distribution near the loss cone (Kennel & Petschek, 1966; Li et al., 2013), the average precipitating electron flux measured within the loss cone by ELFIN CubeSats (Angelopoulos, Tsai, et al., 2020) at low altitude, j_{prec}, can be expressed as a function of the trapped flux measured at an equatorial pitch angle 5% above the loss cone angle α_{LC}, denoted j_{trap} (Mourenas et al., 2023; Mourenas, Zhang, et al., 2022). In the ELFIN data products, j_{prec} is averaged over the loss cone weighted by solid

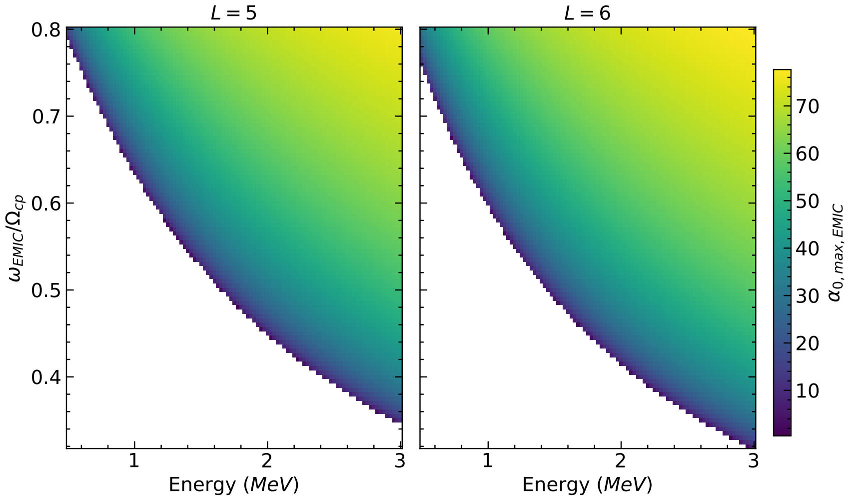

Figure 8. (a) $\alpha_{\max}(\mathrm{EMIC})$ as a function of energy and $\omega_{\mathrm{EMIC}}/\Omega_{\mathrm{cp}}$ at $L = 5$ and $L = 6$ using the empirical model of plasma density inside the plasmasphere from Sheeley et al. (2001).

angle, giving $j_{prec}/j_{trap} \approx 1.3/\left(z_0 + z_0^2/200\right)$ with $z_0 = 2\alpha_{LC}/(\tau_B D_{\alpha\alpha})^{1/2}$ and τ_B the electron bounce period, valid for $j_{prec}/j_{trap} \in [0.001, 0.85]$ (Mourenas et al., 2023). Accordingly, $D_{\alpha\alpha}$ at $\alpha_0 = \alpha_{LC}$ can be inferred from the measured ratio j_{prec}/j_{trap} at ELFIN, giving

$$D_{\alpha\alpha} \approx \frac{\alpha_{LC}^2}{2500\ \tau_B}\left(\sqrt{1+\frac{j_{trap}}{38.5\ j_{prec}}}-1\right)^{-2}, \tag{2}$$

where the above Equation 2 applies for any wave mode in the quasi-linear diffusion regime.

The diffusion rates $D_{\alpha\alpha}$ inferred, using Equation 2, from time-averaged ELFIN measurements of precipitating and trapped electron fluxes (averaged over 10–20 spacecraft spins and taking into account periods without precipitation) are displayed in Figure 9a for different electron energies and different L. We use j_{prec} approximately corrected for atmospheric backscatter in the conjugate region, which is done by subtracting from the measured precipitating flux the upward flux recorded by ELFIN (Mourenas et al., 2021). Note that $D_{\alpha\alpha}$ inferred from ELFIN measurements of j_{prec}/j_{trap} is valid only near 16 MLT, at the location and time of the measurements. Since EMIC waves are likely to be present mainly only at noon-dusk with varying levels of wave power (Meredith et al., 2014; Ross et al., 2021) and less than half of the time, the MLT-averaged and time-averaged diffusion rates should be smaller to much smaller than $\sim 1/8$ of the diffusion rates inferred from the ELFIN measurements in Figure 9a.

For a typical ratio $f_{pe}/f_{ce} \approx 20$ in a noon-dusk plasmaspheric plume at $L \approx 5-6$ (Sheeley et al., 2001; X.-J. Zhang et al., 2016; Ross et al., 2021), one finds that cyclotron resonance is impossible between $0.5-2$ MeV electrons and EMIC waves at the typical frequency $\omega_{\mathrm{EMIC}}/\Omega_{cp} = 0.4$ of peak wave power (Meredith et al., 2014; Kersten et al., 2014; X.-J. Zhang et al., 2016; Ross et al., 2021). However, various works have reported significant low-energy ($\sim 0.3-1$ MeV) electron precipitation by EMIC waves in the noon-dusk sector simultaneously with a much more efficient >1.5 MeV precipitation, similar to ELFIN results displayed in Figure 9 (Angelopoulos et al., 2023; Capannolo et al., 2019; Hendry et al., 2017, 2019). This less efficient low-energy electron precipitation can be explained by quasi-linear electron scattering through cyclotron resonance with a finite tail of high-frequency high-wave-number H-band EMIC waves, of much lower amplitudes than at the peak power frequency $\omega_{\mathrm{EMIC}}/\Omega_{cp} \sim 0.4$ (Angelopoulos et al., 2023), present in Van Allen Probes statistics in the 12–22 MLT sector when $f_{pe}/f_{ce} > 15$ (X.-J. Zhang et al., 2016). This high-frequency wave power tail in the noon-dusk sector, shown in Figure 19a from Angelopoulos et al. (2023), can be approximately fitted as $B_w^2(\omega_{\mathrm{EMIC}}/\Omega_{\mathrm{cp}}) \approx (0.4\ \Omega_{\mathrm{cp}}/\omega_{\mathrm{EMIC}})^7\ B_w^2(\omega_{\mathrm{EMIC}}/\Omega_{\mathrm{cp}} = 0.4)$.

In Figure 9, we check the reliability of this statistical power spectrum fit and of the corresponding analytical estimates of diffusion rates $D_{\alpha\alpha}$, through comparisons with ELFIN observations during the selected event, using a

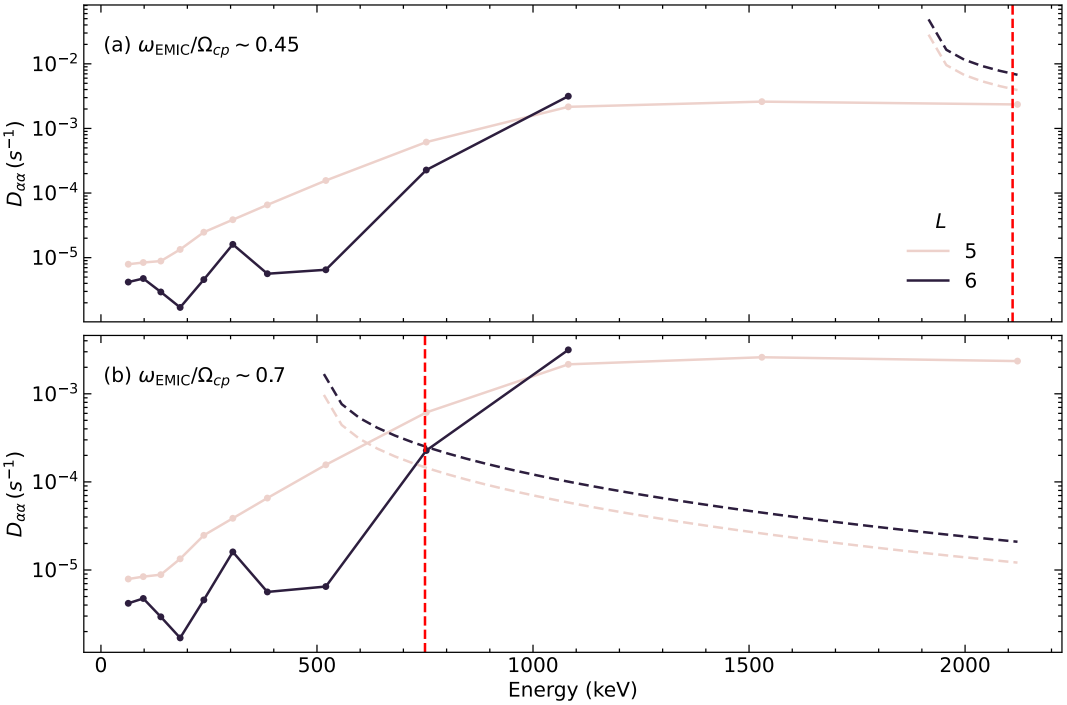

Figure 9. (a) Diffusion rates $D_{\alpha\alpha}$ of electrons near the loss cone inferred, using Equation 2, from ELFIN measurements of precipitating and trapped electron fluxes in the dusk sector near 16 MLT, at $L = 5$ (solid red) and $L = 6$ (solid black) as a function of electron energy E. Diffusion rates $D_{\alpha\alpha}$ near the loss cone evaluated based on analytical estimates for H-band EMIC waves with typical wave and plasma parameters at $L = 5$ (red) and $L = 6$ (black) in a noon-dusk plasmaspheric plume, as a function of energy E are shown (dashed lines) for a typical ratio $f_{pe}/f_{ce} = 20$, a peak wave amplitude of $B_w = 0.5$ nT at $\omega_{\mathrm{EMIC}}/\Omega_{cp} \sim 0.4$, adopting the (minimum) frequency $\omega_{\mathrm{EMIC}}/\Omega_{cp} \sim 0.45$ corresponding to cyclotron resonance with ~2 MeV electrons near the loss cone (the resonant energy is denoted by a red vertical line). (b) Same as (a) with analytical estimates of $D_{\alpha\alpha}$ shown for H-band EMIC waves with a peak wave amplitude of $B_w = 0.5$ nT at $\omega_{\mathrm{EMIC}}/\Omega_{cp} \sim 0.4$ and adopting the (minimum) frequency $\omega_{\mathrm{EMIC}}/\Omega_{cp} \sim 0.7$ corresponding to cyclotron resonance with ~0.75 MeV electrons near the loss cone (the resonant energy is denoted by a red vertical line).

typical ratio $f_{pe}/f_{ce} \sim 20$, and adopting the (minimum) frequency $\omega_{\mathrm{EMIC}}/\Omega_{cp} \sim 0.45$ corresponding to cyclotron resonance with ~2 MeV electrons near the loss cone (the resonant energy is denoted by a red vertical line) in Figure 9(a), and the (minimum) frequency $\omega_{\mathrm{EMIC}}/\Omega_{cp} \sim 0.7$ corresponding to cyclotron resonance with ~0.75 MeV electrons near the loss cone (the resonant energy is denoted by a red vertical line) in Figure 9b. Figures 9a and 9b show analytical estimates (Angelopoulos et al., 2023; Mourenas et al., 2016) of EMIC wave-driven quasi-linear diffusion rates $D_{\alpha\alpha}$ of electrons near the loss cone (dashed lines) calculated with these parameters, using a peak EMIC wave amplitude of $B_w \approx 0.5$ nT at $\omega_{\mathrm{EMIC}}/\Omega_{cp} \sim 0.4$ that allows to roughly recover diffusion rates $D_{\alpha\alpha}$ inferred from ELFIN measurements (solid lines), both at $L = 5$ near 2 MeV in Figure 9a and at $L = 5-6$ near 0.75 MeV in Figure 9b. The stronger statistical EMIC wave power at lower frequency in the adopted statistical wave power spectrum fit explains the stronger diffusion at higher energy (~2 MeV) than at low energy (0.75 MeV) in Figure 9 (note that analytical estimates actually become invalid slightly below the resonant energy indicated by a red vertical line). These results suggest the presence of duskside EMIC wave bursts with peak amplitudes $B_w \approx 0.5$ nT and a low-amplitude tail at high frequencies (Angelopoulos et al., 2023). Taking into account the likely presence of significant temporal and spatial variations of EMIC wave power and frequency spectrum during the selected event, the rough agreement at these two energies between the analytical $D_{\alpha\alpha}$ model (based on statistics of EMIC waves) and ELFIN observations suggests that this simplified model is reliable and can be used for approximately modelling the electron flux evolution during this event.

5.2. Role of Chorus Waves Alone

Energetic electrons of ~10–300 keV injected from the plasma sheet at $L \sim 5-6$ around midnight drift azimuthally toward noon and generate there intense lower-band chorus waves outside the plasmasphere (Li et al., 2010; Meredith et al., 2001; Omura et al., 2008; Tsurutani & Smith, 1974). In turn, such chorus waves can efficiently precipitate low equatorial pitch angle electrons into the atmosphere and energize high equatorial pitch angle electrons up to several MeVs (Horne et al., 2005; Kubota & Omura, 2017; Ma et al., 2016; Omura et al., 2007; Thorne et al., 2013). Although chorus waves mainly consist of wave packets of relatively high amplitudes (SantolíK et al., 2003; Santolík et al., 2014) that can reach the threshold for nonlinear interaction (X. J. Zhang et al., 2019), most chorus packets are relatively short and separated by strong and random wave frequency and phase jumps (X. J. Zhang, Mourenas, et al., 2020; X. J. Zhang, Agapitov, et al., 2020), allowing an approximate quasilinear diffusive treatment (Artemyev et al., 2022; Gan et al., 2022; Z. An et al., 2022).

A simplified analytical expression (validated vs. numerical calculations) for the pitch angle diffusion rate $D_{\alpha\alpha}$ of relativistic electrons ($\sim 0.1-1$ MeV) near the loss cone by quasi-parallel lower-band chorus waves is (Agapitov et al., 2019; Mourenas, Artemyev, Agapitov, & Krasnoselskikh, 2014):

$$D_{\alpha\alpha}\left[\mathrm{s}^{-1}\right] \approx \frac{B_w^2\,\Omega_{ce}^{4/3}}{1400\,\Omega_{pe}^{14/9}\,\omega_{ch}^{7/9}\,(2E+1)\left(E^2+E\right)^{7/9}\,\cos^2\alpha_0}, \tag{3}$$

with E in MeV, α_0 the equatorial pitch angle, B_w^2 in pT^2 and $\omega_{ch}/\Omega_{ce} \sim 0.15$ the MLT-averaged wave power and normalized chorus frequency at magnetic latitudes $\lambda \in [10°, 35°]$ of cyclotron resonance with $\sim 0.1-2$ MeV electrons near the loss cone (Agapitov et al., 2018; Mourenas et al., 2021). The corresponding electron lifetime is approximately given by $\tau_L \approx 1/(2D_{\alpha\alpha})$ above 100 keV as $D_{\alpha\alpha}\tan\alpha_0$ has a minimum at low equatorial pitch angles α_0 (Albert & Shprits, 2009; Aryan et al., 2020; Mourenas, Artemyev, Agapitov, & Krasnoselskikh, 2014). The bounce- and MLT-averaged energy diffusion rate of relativistic electrons at $\alpha > 60°$ can be similarly written as (Agapitov et al., 2019; Mourenas, Artemyev, Agapitov, & Krasnoselskikh, 2014; Mourenas et al., 2012):

$$\frac{D_{EE}}{E^2}\left[\mathrm{s}^{-1}\right] \approx \frac{B_w^2\,\Omega_{ce}^{3/2}\,\omega_{ch}^{1/2}\,(E+1)^{1/2}\,\Xi(E)}{190\,\Omega_{pe}^{3}\,(1+2E)\,E^{3/2}}, \tag{4}$$

with B_w^2 in pT^2, E in MeV, $\Xi(E) \approx (\min(E,1))^{1/2}$ a factor allowing to approximately recover full numerical calculations of D_{EE} for $E \in [0.1, 2]$ MeV (Agapitov et al., 2018, 2019), and $\omega_{ch}/\Omega_{ce} \sim 0.3$ the MLT-averaged parallel chorus wave power and frequency at latitudes $\lambda < 10°$ (Agapitov et al., 2018; Li et al., 2016).

Figure 10 shows typical whistler-mode wave spectra measured during the investigated event by the ERG spacecraft (Miyoshi, Shinohara, Takashima, et al., 2018; Y. Kasahara, Kasaba, et al., 2018) at latitudes $\sim 0° - 3°$ and $L \sim 5-6$. Strong lower-band chorus waves are seen from 2 UT on 17 April 2021, to 2021 UT on April 17. The MLT- and time-averaged diffusion rates $D_{\alpha\alpha}$ and D_{EE} of electrons by chorus waves have been estimated based on ERG measurements of chorus wave power and frequency, using Equations 3 and 4, and also adopting the typical mean frequency of chorus waves at low latitudes for D_{EE}, and at middle latitudes for $D_{\alpha\alpha}$ (Agapitov et al., 2018), corresponding to cyclotron resonance with high and low equatorial pitch-angle electrons, respectively (Mourenas et al., 2023). They are displayed in Figure 11.

5.3. Combined Roles of EMIC and Chorus Waves in Different MLT Sectors

First, it is worth noting that in a simplified modelling of a slow diffusive electron transport in phase space, the effects on electron flux of diffusive electron precipitation loss and energization can be averaged over an event duration, and both assumed to occur during this whole event, because these diffusive processes can be simply averaged over such long time scales—and therefore also over MLT, which corresponds to an average over the azimuthal drift period of electrons—without loss of long-term accuracy concerning the effects on trapped fluxes (e.g., see Ross et al., 2019; Shprits et al., 2009). These diffusive processes do not need to be continuously or simultaneously present at all times during the actual event for such a simplified modelling to be relevant: for instance, they may occur at different locations, and they may each occur during short successive periods, provided that the time intervals between these separate periods of activity be shorter than the typical time scales of electron diffusive energization and loss during this event.

Based on Van Allen Probes statistics, H-band EMIC waves excited in the noon-dusk sector often reach a wave power similar to or higher than chorus waves excited in low plasma density regions in the night/dawn sector (X.-J.

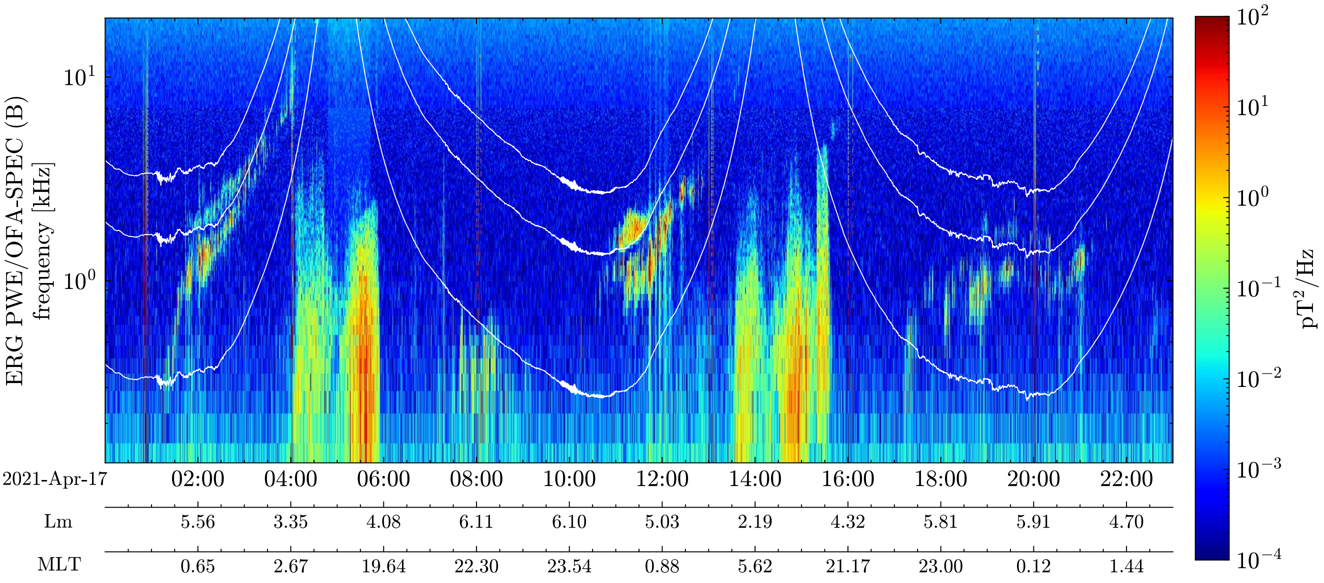

Figure 10. Whistler-mode wave spectra measured by ERG spacecraft during the investigated event. White curves show (from bottom to top) $0.1f_{ce}$, $0.5f_{ce}$, f_{ce}.

Zhang et al., 2016; Agapitov et al., 2018, 2019; Ross et al., 2021). These two types of waves can frequently be observed contemporaneously on the same L-shells in these two MLT sectors (X.-J. Zhang et al., 2017), because injections from the plasma sheet provide anisotropic electron and ion populations, respectively, generating chorus and EMIC waves (e.g., Birn et al., 1996; Birn et al., 2014; Gabrielse et al., 2014; Tao et al., 2011; Ukhorskiy et al., 2022).

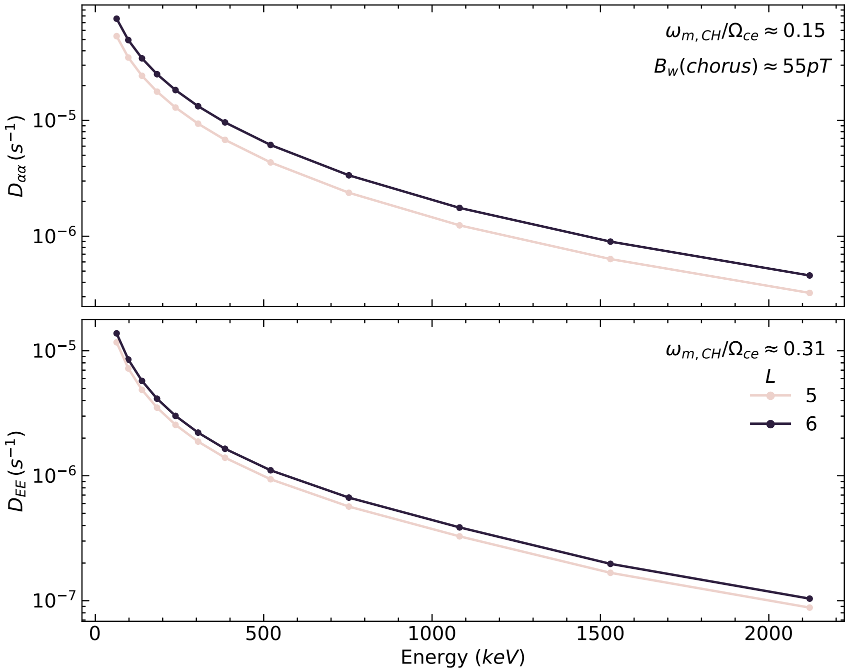

Figure 11. Chorus wave-driven electron quasi-linear pitch angle and energy diffusion rates $D_{\alpha\alpha}(CH)$ and $D_{EE}(CH)/E^2$ as a function of energy at $L = 5$ and 6, MLT-averaged based on ERG chorus wave data during this event (assuming a typical MLT distribution of chorus power, see (Agapitov et al., 2018), adopting an empirical plasma density model outside the plasmasphere. Here, chorus wave power is assumed constant at latitudes $\sim 0^\circ - 30^\circ$ to first order.

The combined effects of EMIC and chorus waves can lead to stronger and faster losses (in less than $\sim 0.5-1$ day) of trapped electron flux at $>1.5-2$ MeV than when considering either wave mode alone (Li et al., 2007; Mourenas et al., 2016, 2021; Boynton et al., 2017; X.-J. Zhang et al., 2017; Drozdov et al., 2020). However, this requires an initial electron flux that decreases more slowly as a function of energy than its asymptotic steady-state energy spectrum for given EMIC and chorus wave power and frequency distributions (Mourenas, Artemyev, et al., 2022a; Mourenas et al., 2023). In such a situation, the main effect of EMIC waves is to quickly precipitate low equatorial pitch angle electrons into the atmosphere, an effect equivalent to a widening of the effective loss cone for subsequent chorus-driven electron pitch angle diffusion, leading to a strong reduction of electron lifetimes above ~ 1.5 MeV compared to lifetimes in the absence of EMIC waves (Mourenas et al., 2016; Mourenas et al., 2021; X.-J. Zhang et al., 2017).

Such fast electron losses typically require H-band EMIC waves with a time- and MLT-averaged power $\langle B^2_{w,EMIC}\rangle$ near the equator larger than the average chorus power $\langle B^2_{w,chorus}\rangle$ at middle latitudes (where chorus wave cyclotron resonance with electrons near the loss cone occurs), a sufficiently high $\omega_{\mathrm{EMIC}}/\Omega_{\mathrm{cp}} > 0.45$, and a sufficiently high ratio $f_{pe}/f_{ce} > 15$ in the dusk region where EMIC waves are present (Mourenas et al., 2016; X.-J. Zhang et al., 2017). To prevent an initial, or subsequent, increase of electron flux due to chorus wave-driven electron energization (Agapitov et al., 2019; Horne et al., 2005; Mourenas et al., 2012; Summers et al., 1998), the MLT-averaged chorus wave power at low latitudes must not be too large compared to the MLT-averaged EMIC wave power, and f_{pe}/f_{ce} must not be too low (typically $>4-5$) in the 23-10 MLT sector where low-latitude chorus waves are most intense (Mourenas, Artemyev, et al., 2022a).

The time-averaged and MLT-averaged H-band EMIC wave power at the frequency of peak power is expected to be roughly $B^2_w(\omega_{\mathrm{EMIC}}/\Omega_{\mathrm{cp}} = 0.4) \sim 0.001\ \mathrm{nT}^2$ at $L \sim 5-6$ based on Van Allen Probes statistics when $Pdyn \simeq 3$nPa as during the present event (Ross et al., 2021), and the local plasma density in the duskside high-density plasmaspheric plume region is given by an empirical model (Sheeley et al., 2001). The low intensity H-band EMIC waves present at $\omega_{\mathrm{EMIC}}/\Omega_{\mathrm{cp}} > 0.4$ when $f_{pe}/f_{ce} > 15$ in the dusk sector in Van Allen Probes statistics (X.-J. Zhang et al., 2016; Angelopoulos et al., 2023) are taken into account by using the EMIC wave-driven pitch angle diffusion rate near the loss cone $D_{\alpha\alpha}$(EMIC) inferred from ELFIN measurements in Figure 9 during this event at 16 MLT, multiplied by a factor $\sim 0.001/0.5^2 = 1/250$ to agree with the statistical MLT-averaged and time-averaged EMIC wave power. The time-averaged lower-band chorus wave power is taken as $B^2_w \sim 0.003\ \mathrm{nT}^2$ at the equator and $L \sim 5-6$ based on spacecraft statistics (Agapitov et al., 2018) in agreement with ERG (Arase) measurements during this event, and the local plasma density in the dawn sector is given by an empirical trough density model (Sheeley et al., 2001). The decrease in MLT- and time-averaged chorus wave power from the equator to higher latitudes in statistical observations (Agapitov et al., 2018) is taken into account in $D_{\alpha\alpha}$(chorus) via an approximate factor $\xi(E) = B^2_w(\lambda)/B^2_w(\lambda < 10°) \approx \max\left(0.08, \sqrt{0.06/\left(E + 6E^5\right)}\right)$ as a function of the energy $E \in [0.06, 2]$ MeV of electrons near the loss cone in cyclotron resonance with such chorus waves (Mourenas et al., 2023). This allows us to refine the electron lifetime formulas provided by Mourenas et al. (2016) and X.-J. Zhang et al. (2017) in the presence of contemporaneous EMIC and chorus waves in the high-density dusk sector and in the low-density dawn sector, respectively.

Using electron pitch angle diffusion rates for chorus waves from Equation 3 and for H-band EMIC waves from Equation 1 in (Mourenas et al., 2016) corrected at low energy as detailed above, and taking into account the H-band EMIC wave power tail at high frequency (X.-J. Zhang et al., 2016; Angelopoulos et al., 2023), the total diffusion rate at each pitch angle is $\langle D_{\alpha\alpha}\rangle \approx D_{\alpha\alpha}(\mathrm{chorus}) + D_{\alpha\alpha}(\mathrm{EMIC})$. The corresponding electron lifetime τ_L can be estimated as (Albert & Shprits, 2009; Mourenas, Artemyev, et al., 2022a; Mourenas et al., 2016):

$$\tau_L(E) \approx \int_{\alpha_{0,LC}}^{\alpha_{0,\max}} \frac{d\alpha_0}{4\,\langle D_{\alpha\alpha}(\alpha_0)\rangle \tan\alpha_0}, \qquad (5)$$

with $\alpha_{0,LC}$ the equatorial loss cone angle and $\alpha_{0,\max} \sim 80°-85°$ the typical maximum pitch angle of cyclotron resonance with lower-band chorus waves of high frequencies (Agapitov et al., 2018; Mourenas et al., 2016). Here, the main contribution to the integral in Equation 5 at $E \sim 0.1-2$ MeV usually comes from low to moderate equatorial pitch angles, allowing us to use the approximation $\tau_L(E) \approx 0.5/\langle D_{\alpha\alpha}(\alpha_{0,LC})\rangle$ (Albert & Shprits, 2009).

In the presence of sustained energetic electron injections at 0.05 MeV $\leq E \leq 0.15$ MeV and significant energy diffusion by chorus waves and pitch angle diffusion by chorus and EMIC waves, it has been shown both numerically and analytically (Hua et al., 2022; Mourenas, Artemyev, et al., 2022a; Mourenas et al., 2023) that the normalized electron flux energy spectrum should rapidly tend toward a steady-state attractor $J_{UL}(E)$. Physically, this evolution of $J(E,t)$ toward the energy spectrum shape of the steady-state attractor $J_{UL}(E)$ can be explained as follows (Mourenas et al., 2023): since a steeper negative gradient $\partial \mathrm{PSD}(E)/\partial E$ of the electron phase space density (PSD) leads to a faster electron transport through chorus wave-driven diffusive energization toward the region of initially lower PSD at higher E (Schulz & Lanzerotti, 1974), the gradient $\partial \mathrm{PSD}(E,t)/\partial E$ will progressively adjust itself to tune the net incoming electron flow at each energy E (due to chorus wave-driven energization of lower-energy electrons), until it exactly compensates electron loss at this same energy E (due to chorus and EMIC wave-driven pitch-angle diffusion toward the loss cone and also chorus wave-driven electron acceleration toward higher E). Therefore, the initial gradient, $\partial J(E,t_0)/\partial E$, determined by the strength of injections at low energy, will control the evolution of $J(E,t)$ during the following hours (see schematic view in Figure 7). If the initial flux decreases toward high E slower than the steady-state attractor $J_{UL}(E)$, chorus wave-driven energization will be inefficient due to the weakly negative PSD gradient $\partial \mathrm{PSD}(E,t)/\partial E$, and since it will not be able to transport a sufficient quantity of electrons to high E for replacing all such electrons lost through precipitation, $J(E,t)$ will drop at high E (see Figure 7, bottom left) to assume this attractor shape (Mourenas et al., 2016, 2023). But if the initial flux decreases faster than $J_{UL}(E)$, chorus wave-driven energization will be stronger due to the steep negative PSD gradient, and since it will transport a larger number of electrons to high E than the number of such high E electrons lost via precipitation, $J(E,t)$ will increase at high E (see Figure 7, bottom right) to assume the attractor shape (Mourenas et al., 2023).

The steady-state attractor shape $J_{UL}(E)$ can be calculated numerically, by solving the corresponding simplified Fokker-Planck diffusion equation, using $\tau_L(E)$ from Equation 5 and $D_{EE}(E)$ from Equation 4 (Mourenas, Artemyev, et al., 2022a; Mourenas et al., 2023). Alternatively, one can use the approximate analytical solution (validated by numerical simulations) obtained by Mourenas et al. (2023):

$$J_{UL}(E) \approx A \cdot \left[(1+2E)\left(E^2+E\right)\right]^{1/2} \cdot I_{\frac{1}{2}}\left(\frac{\sqrt{\epsilon\, K-R}}{4E+2}\right), \tag{6}$$

with A a normalization constant, I_z the modified Bessel function of the first kind, $K = 20 + 13\,E^2 + 0.06/E^2$, $R = 4 + 1/E^{3/2}$, $\epsilon(E) = E^{5/4}(E+1)^{5/4}/(D_{EE}(E)\,\tau_L(E))$, where $\tau_L(E)$ is taken to first order as $\tau_L(E) \approx 0.5/\langle D_{\alpha\alpha}(\alpha_{0,LC})\rangle$ using $\langle D_{\alpha\alpha}\rangle \approx D_{\alpha\alpha}(\mathrm{chorus}) + D_{\alpha\alpha}(\mathrm{EMIC})$ using $\xi(E)$ to estimate chorus power at the latitude of resonance based on its average equatorial power $B_w^2 \sim 0.003$ nT^2, $D_{EE}(E)$ is given by Equation 4 using the equatorial average chorus wave power, and E is in MeV. The corresponding $\epsilon(E)$ for chorus waves alone has also been derived in a previous work (Mourenas et al., 2023). Note that $J_{UL}(E)$ provided in Equation 6 is a discontinuous solution, which has to be calculated separately over each E-bin and renormalized at each E-bin start, with constant K, R, $\epsilon(E)$ values inside each bin (see details in Mourenas et al., 2023). Chorus waves are present in the plasma trough in the dawn sector, while EMIC waves are dominant within a plasmaspheric plume with corresponding plasma densities taken from empirical models (Sheeley et al., 2001).

Let us emphasize that the energy gradient $\partial J_{UL}(E)/\partial E$ of the steady-state attractor flux directly depends on the $\epsilon(E)$ factor: a smaller $\epsilon(E)$ leads to a weaker gradient (Mourenas, Artemyev, et al., 2022a; Mourenas et al., 2023). A smaller ϵ corresponds to a larger chorus wave-driven energy diffusion rate D_{EE} and/or a longer electron lifetime τ_L, that is, it corresponds to a stronger chorus wave power at low latitudes (where resonant electron energization by chorus waves occurs) than at high latitudes (where chorus waves resonantly scatter electrons in pitch-angle toward the loss cone), and also comparatively less EMIC wave power (since EMIC waves can help reduce the net electron lifetime compared to a situation with chorus waves alone).

Figure 12 shows electron flux energy spectra measured at different times on 17 April 2021 at $L \sim 5-6$ (black to magenta curves), by ERG near the magnetic equator (panel a) and by ELFIN at low altitude (panel b), and projected to the equator (i.e., to equatorial pitch angles $\alpha_0 = 90°$) by assuming a typical distribution shape $J(\alpha_0 = 90°)/J(\alpha_0) \approx 1/\sin\alpha_0$ (R. Shi et al., 2016), with $\sin\alpha_0 \approx (B(\lambda = 0°)/B(\lambda))^{1/2}$ and $B(\lambda)$ the geomagnetic field strength at the latitude λ of flux measurement. ERG latitudes of measurements $\lambda < 30°$ correspond to a

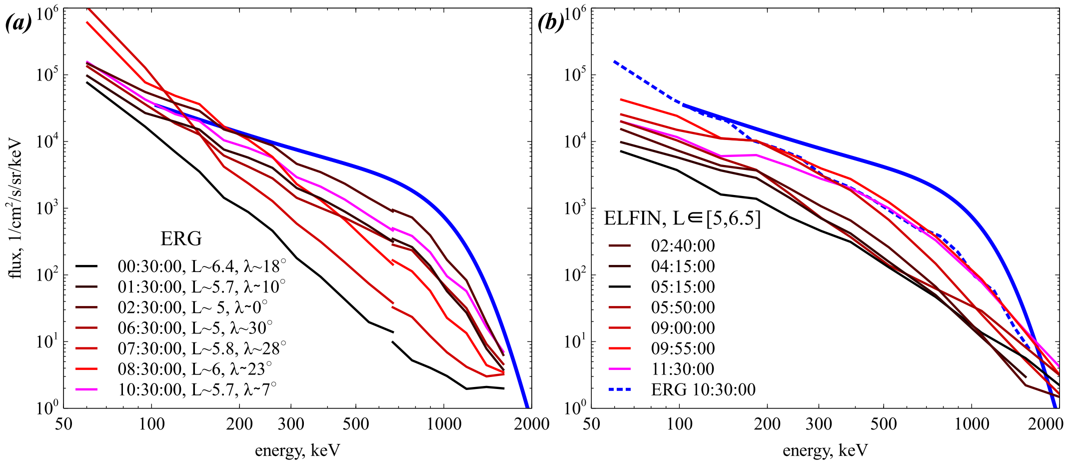

Figure 12. (a) Trapped electron flux energy spectra $J(\alpha_0 = 90^\circ, E)$ (black to magenta curves) measured by ERG near the magnetic equator at different times on 17 April 2021, and projected to the equator by assuming a typical shape $J(\alpha_0 = 90^\circ)/J(\alpha_0) \approx 1/\sin\alpha_0$, with $\sin\alpha_0 \approx (B(\lambda = 0^\circ)/B(\lambda))^{1/2}$ and $B(\lambda)$ the geomagnetic field strength at the latitude of measurement. The approximate steady-state spectrum shape $J_{UL}(E)$ expected to be reached asymptotically in time in the presence of both EMIC and chorus wave-driven pitch angle and energy diffusion is also shown (blue curve), normalized at the measured flux level at 100 keV and 10:30 UT. (b) Same as (a) but showing trapped electron flux energy spectra $J(\alpha_0 = 90^\circ, E)$ (black to magenta curves) measured by ELFIN at low altitude at different times and projected to the equator. Two curves from panel (a) are reproduced for the sake comparison: $J(\alpha_0 = 90^\circ, E)$ inferred from ERG data at 10:30 UT (dashed blue) and $J_{UL}(E)$ normalized to ERG flux at 100 keV and 10:30 UT (solid blue).

measured $\alpha_0 \gtrsim 35^\circ$. At $L > 5$, trapped electron fluxes usually vary coherently with fluxes at $\alpha_0 = 90^\circ$ (Mourenas et al., 2021, 2023; Shane et al., 2023). This is confirmed by similarity between trapped equatorial fluxes $J(\alpha_0 = 90^\circ)$ of $100 - 2000$ keV electrons at $9:55 - 11:30$ UT and $L \simeq 5 - 6$ inferred from near-equatorial ERG measurements at $\alpha_0 \simeq 77^\circ$ in Figure 12a and inferred from high-latitude ELFIN measurements at $\alpha_0 \approx 3^\circ$ in Figure 12b (compare the dashed blue curve with solid red and magenta curves in panel (b)). The similarity of inferred fluxes $J(\alpha_0 = 90^\circ)$ at $1 - 2$ MeV further indicates that $\langle D_{\alpha\alpha}(\alpha_0)\rangle \tan\alpha_0$ has a minimum at low α_0, and no deeper minimum at $\alpha_0 \sim 45^\circ - 70^\circ$. A deeper minimum at $\alpha_0 \sim 45^\circ - 70^\circ$ would indeed have led to a strong drop of $J(\alpha_0)$ from $\alpha_0 \simeq 77^\circ$ to $\alpha_0 \simeq 30^\circ$ (Mourenas, Artemyev, Agapitov, Krasnoselskikh, & Li, 2014) and a much smaller $J(\alpha_0 = 90^\circ)$ inferred from ELFIN than $J(\alpha_0 = 90^\circ)$ inferred from ERG. This is consistent with an EMIC wave power spectrum with a tail that extends to high frequencies as in statistical observations (X.-J. Zhang et al., 2016; Angelopoulos et al., 2023).

On 17 April 2021, *Dst* varied from −38 nT at 0–2 UT to −24 nT at 11–12 UT, reaching a minimum of ~ -50 nT at 4–7 UT, indicating a weak *Dst*-effect on trapped fluxes at $L < 6$ (H.-J. Kim & Chan, 1997), much weaker than the effect of injections and the ensuing chorus-driven electron acceleration. In addition, the Last Closed Drift Shell (LCDS) has been calculated using the LANL* neural network (Yu et al., 2012) with the TS04 magnetic field model (Tsyganenko & Sitnov, 2005). It decreased to $L(LCDS) \simeq 6.1 - 6.2$ at 2–5 UT, but increased back to $L(LCDS) \simeq 6.5 - 7.0$ at 5:30-11:30 UT. This implies that the outward electron loss was likely limited to $L > 6.1$ at 2–5 UT and to $L \geq 6.5$ after 5:30 UT during this event.

The average $Kp \sim 4.2$ between 6 UT and 11 UT suggests a possible simultaneous presence of electron radial diffusion by ULF waves, but with a moderate statistical electric radial diffusion rate, $D_{LL} \sim 1.7$ day^{-1} at $L \simeq 6$ (Ozeke et al., 2014). The ULF wave-driven inward radial PSD shift can be written as $\Delta L \approx (\Delta t\, D_{LL})\partial \ln(PSD)/\partial L$ (Schulz & Lanzerotti, 1974). Consequently, a very large positive initial outward electron phase space density (PSD) gradient $\partial PSD/\partial L$ at first adiabatic invariant $\mu \sim 300 - 1000$ MeV/G would have been needed over $L = 5.5 - 6.5$ (below the LCDS) to produce in $\Delta t \sim 3$ hours the $0.5 - 1$ MeV electron flux increase by a factor of ≈ 10 observed by ERG and ELFIN between ~ 7 UT and 10 UT at $L \sim 5.7$. The presence of such a steep positive PSD gradient seems unlikely, due to the low $L(LCDS) \simeq 6.5 - 7.0$ simultaneously driving outward electron losses at $L \geq 6.5$. Although GOES measurements at $L \sim 7.7$ show significant injections of $\approx 600 - 900$ keV electrons after 7 UT (see Figure 2), the LCDS then remained at $L(LCDS) \simeq 6.5 - 7.0$. This suggests that these electrons, azimuthally drifting on open drift shells, should have been more rapidly lost to the outer space than scattered inward to $L \sim 5.8$, except if ULF wave power was much larger than in statistical averages for the considered Kp or in the presence of significant drift orbit bifurcations (Ukhorskiy et al., 2011). Therefore, although one cannot fully exclude an important effect of inward radial diffusion of such electrons, this effect is not expected to have been dominant in the observed electron flux enhancement at $L \simeq 5.8$ during this weak storm.

The above-discussed theoretical steady-state attractor $J_{UL}(E)$ from Equation 6 is also shown (solid blue curve) in Figures 12a and 12b, normalized at 100 keV to the latest equatorial trapped flux inferred from ERG data around 10:30 UT. It represents the hardest trapped electron flux energy spectrum that can theoretically be reached during sufficiently strong and sustained injections in the presence of both EMIC and chorus wave-driven electron pitch angle and energy diffusion (Hua et al., 2022; Mourenas, Artemyev, et al., 2022a; Mourenas et al., 2023). The reduction of the lifetime of low-energy electrons at 0.3–1 MeV by the high-frequency wave power tail of H-band EMIC waves (Angelopoulos et al., 2023) leads to a slightly faster decrease of $J_{UL}(E)$ over $0.4-1.0$ MeV than in previous calculations where this tail was neglected to the first order (Mourenas, Artemyev, et al., 2022a; Mourenas et al., 2023).

The equatorial trapped fluxes inferred from ERG and ELFIN measurements near the end of this event, at 10–11 UT (magenta curves), decrease slightly faster toward higher energy than the upper limit spectrum $J_{UL}(E)$ in Figures 12a and 12b). This implies that the dynamical system did not yet reach this limiting energy-spectrum shape, probably due to too weak time-integrated injections and chorus wave-driven electron energization. In such a situation, over time scales larger than $\sim 5-10$ hours, the electron flux is expected to increase above $0.5-1$ MeV despite the precipitation loss driven by EMIC waves, due to a strong electron acceleration by chorus waves in the presence of both a steeply decreasing PSD gradient toward higher energy and a roughly fixed low energy boundary of the flux energy spectrum maintained by the $\sim 100-300$ keV seed electron injections observed by GOES (Mourenas, Artemyev, et al., 2022a; Mourenas et al., 2023). The initial steep negative PSD gradient toward higher energy should indeed boost the efficiency of chorus wave-driven energy diffusion of electrons toward the domain of lower PSD at higher E (Schulz & Lanzerotti, 1974; Walt, 1994), allowing it to transport more electrons at high E than the number of such high E electrons lost via EMIC wave-driven precipitation, leading to an increase of $J(E,t)$ at high E (see Figure 7, bottom right) as $J(E,t)$ tends toward the upper limit attractor $J_{UL}(E)$ (Mourenas et al., 2023). But only after a sufficiently long period of sustained injections is it expected that the trapped flux $J(E)$ reaches a slope similar to that of the asymptotic spectrum $J_{UL}(E)$.

A fast dropout of $>1-2$ MeV electron flux up to high equatorial pitch angles, due to combined pitch angle scattering by chorus and EMIC waves, can instead occur (see Figure 7, bottom left, and the work by Mourenas et al., 2024), but only when the trapped flux $J(E)$ decreases with energy less fast than the steady-state spectrum $J_{UL}(E)$ (Mourenas, Artemyev, et al., 2022a; Mourenas et al., 2023), in particular over short time scales, $<3-5$ hours, when chorus wave-driven energization has not yet efficiently transported low-energy electrons to such high energies (Mourenas et al., 2016, 2024).

During the present event, one cannot fully exclude another possible scenario: additional electron loss via outward radial diffusion to the LCDS (Olifer et al., 2018; Pinto et al., 2020; Shprits, Thorne, Friedel, et al., 2006; Turner, Angelopoulos, et al., 2012; Turner et al., 2014) could have increased electron loss compared to the sole EMIC and chorus wave-driven precipitation loss into the atmosphere, potentially leading to an asymptotic spectrum decreasing faster with E than the estimate $J_{UL}(E)$ calculated in the absence of such additional losses. However, fast outward electron loss at $L = 4.2-6.6$ is statistically much less frequent and weaker below $\sim 500-800$ keV than above $\sim 500-800$ keV (Boynton et al., 2016, 2017; Turner, Angelopoulos, et al., 2012), whereas Figure 12 shows that the faster decrease of measured fluxes than $J_{UL}(E)$ occurs mainly below 500–800 keV.

After such an event, once substorm activity has subsided and ion and electron injections have become much less significant, the trapped electron flux $J(E,t)$ should decrease and slowly tend toward a different, quiet-time attractor, $J_{UL,quiet}(E)$, which should usually decrease faster toward higher energy than the above-discussed active-time attractor $J_{UL}(E)$. As noted before, the gradient $\partial J_{UL,quiet}/\partial E$ of the attractor depends on the factor ϵ, which varies like $\approx 1/(D_{EE}\tau_L)$. During quiet times, EMIC wave power decreases compared to active times, increasing the lifetime τ_L, and the MLT-averaged chorus wave power at low latitudes decreases compared to active times, and more strongly than at high latitudes (Agapitov et al., 2018), decreasing more significantly the chorus wave-driven D_{EE} than the chorus wave-driven $D_{\alpha\alpha}$, and further increasing ϵ compared to active times. This leads to a steeper negative gradient $\partial J_{UL,quiet}/\partial E$ than during active times, probably explaining the steep negative energy gradient of the observed initial flux $J(E)$ in Figure 12a at 0:30 UT (black curve). A sudden dropout of electron flux through magnetopause shadowing would also decrease more strongly $J(E,t)$ above 500–800 keV than at lower energy, compared to the final $J(E,t)$ reached during the preceding active times (Boynton et al., 2016; Turner, Angelopoulos, et al., 2012).

6. Discussion and Conclusions

In this study, we examined a particular event on 17 April 2021 characterized by a series of strong electron and ion injections, significant electron precipitation driven by EMIC and chorus waves, and electron acceleration mainly attributable to chorus waves. During this event, GOES, Van Allen Probes, ERG (ARASE) and MMS spacecraft have measured waves and trapped particle fluxes at high altitude near the magnetic equator, while ELFIN and POES spacecraft have recorded trapped and precipitating particle fluxes at low altitude, providing sufficient data to enable a thorough analysis of the involved physical phenomena.

Despite observations by ELFIN and POES indicating effective precipitation of electrons in the $\sim 0.1-1.5$ MeV range in the outer radiation belt due to EMIC and chorus waves, an increase in trapped electron fluxes was observed across nearly all energy ranges. Combining theoretical estimates of electron quasi-linear pitch angle and energy diffusion by chorus and EMIC waves with statistics of wave power distribution, we have shown that long-lasting electron losses driven by EMIC waves may not deplete $\sim 0.1-1.5$ MeV electron fluxes in the outer radiation belt over the long run (>8 hours) when a sufficiently negative derivative $\partial f/\partial E<0$ of the electron PSD $f(E)$ is present. A sufficiently negative PSD gradient may, in fact, permit the strong transport of lower-energy injected electrons to higher energies via chorus wave-driven acceleration, thus more than compensating for potential losses of relativistic electrons due to EMIC and chorus wave-induced precipitation into the atmosphere (Mourenas, Artemyev, et al., 2022a; Mourenas et al., 2023). Electron injections, measured near $L\approx 7$ by GOES, were sufficiently strong after 7 UT to provide the large amount of $\sim 60-200$ keV seed electrons needed that were subsequently accelerated by chorus waves to progressively higher energies (Hua et al., 2022; Mourenas et al., 2023), compensating for electron losses due to wave-driven electron precipitation below ~ 1.5 MeV at $L=5-6.5$. Together with some possible direct injections of relativistic electrons at 0.5–1 MeV and/or inward radial diffusion by ULF waves (associated with adiabatic electron heating to 0.5–1 MeV), this ultimately led to a net increase of relativistic electron fluxes.

This case study therefore underlines the fact that strong EMIC and chorus wave-driven electron losses do not necessarily correspond to a simultaneous decrease of trapped electron fluxes. Sufficiently strong injections and chorus wave-driven electron acceleration in the presence of a sufficiently steep negative electron energy PSD gradient can balance such wave-driven losses. As such, all of these factors should be integrated into global simulation models for an accurate reconstruction of the evolution of trapped electron fluxes.

Data Availability Statement

ELFIN data is available at https://elfin.igpp.ucla.edu. Science data of the ERG (Arase) satellite were obtained from the ERG Science Center operated by ISAS/JAXA and ISEE/Nagoya University (https://ergsc.isee.nagoya-u.ac.jp/index.shtml.en, Miyoshi, Hori, et al. (2018)). The present study analyzed the HEP L2_v03_01 data (Mitani, Hori, et al., 2018), MEPe L2_v01_02 data (S. Kasahara, Yokota, Hori, et al., 2018), MGF L2_v04_04 data (Matsuoka, Teramoto, Imajo, et al., 2018), ORB L2_v03 data (Miyoshi, Shinohara, & Jun 2018), PWE OFA L2.v02_03 data (Y. Kasahara, Kojima, et al., 2018). Data was retrieved and analyzed using PySPEDAS and SPEDAS (Angelopoulos et al., 2019). Code used for the analysis is available in the GitHub repository https://github.com/Beforerr/EMIC_multi-satellites_study.

Acknowledgments
Z.Z., X.J.Z., A.V.A., and V.A. acknowledge support by NASA awards 80NSSC23K0108, 80NSSC23K0403, 80NSSC23K1038, and NSF Grants AGS-1242918, AGS-2019950, and AGS-2021749. Y. M. acknowledge support by JSPS-Grant 23H01229, 22KK0046, 22H00173, 21H04526, 22K21345. We are grateful to NASA's CubeSat Launch Initiative for the successful launch of ELFIN. We acknowledge early support of ELFIN project by the AFOSR, under its University Nanosat Program, UNP-8 project, contract FA9453-12-D-0285, and by the California Space Grant program. We acknowledge critical contributions of numerous volunteer ELFIN team student members.

References

Adair, L., Angelopoulos, V., Sibeck, D., & Zhang, X.-J. (2022). A statistical examination of EMIC wave-driven electron pitch angle scattering signatures. *Journal of Geophysical Research*, *127*(2), e2021JA029790. https://doi.org/10.1029/2021JA029790

Agapitov, O. V., Mourenas, D., Artemyev, A., Hospodarsky, G., & Bonnell, J. W. (2019). Time scales for electron quasi-linear diffusion by lower-band chorus waves: The effects of {{\omega}}_{pe}/{{\upOmega}}_{ce} dependence on geomagnetic activity. *Geophysical Research Letters*, *46*(12), 6178–6187. https://doi.org/10.1029/2019GL083446

Agapitov, O. V., Mourenas, D., Artemyev, A. V., Mozer, F. S., Hospodarsky, G., Bonnell, J., & Krasnoselskikh, V. (2018). Synthetic empirical chorus wave model from combined van allen probes and cluster statistics. *Journal of Geophysical Research (Space Physics)*, *123*(1), 297–314. https://doi.org/10.1002/2017JA024843

Albert, J. M. (2003). Evaluation of quasi-linear diffusion coefficients for EMIC waves in a multispecies plasma. *Journal of Geophysical Research (Space Physics)*, *108*(A6), 1249. https://doi.org/10.1029/2002JA009792

Albert, J. M., & Bortnik, J. (2009). Nonlinear interaction of radiation belt electrons with electromagnetic ion cyclotron waves. *Geophysical Research Letters*, *36*(12), 12110. https://doi.org/10.1029/2009GL038904

Albert, J. M., Selesnick, R. S., Morley, S. K., Henderson, M. G., & Kellerman, A. C. (2018). Calculation of Last closed drift shells for the 2013 GEM radiation belt challenge events. *Journal of Geophysical Research*, *123*(11), 9597–9611. https://doi.org/10.1029/2018JA025991

Albert, J. M., & Shprits, Y. Y. (2009). Estimates of lifetimes against pitch angle diffusion. *Journal of Atmospheric and Solar-Terrestrial Physics*, *71*(16), 1647–1652. https://doi.org/10.1016/j.jastp.2008.07.004

Allison, H. J., & Shprits, Y. Y. (2020). Local heating of radiation belt electrons to ultra-relativistic energies. *Nature Communications*, *11*(1), 4533. https://doi.org/10.1038/s41467-020-18053-z

An, X., Artemyev, A., Angelopoulos, V., Zhang, X., Mourenas, D., & Bortnik, J. (2022a). Nonresonant scattering of relativistic electrons by electromagnetic ion cyclotron waves in Earth's radiation belts. *Physical Review Letters*, *129*(13), 135101. https://doi.org/10.1103/PhysRevLett.129.135101

An, Z., Wu, Y., & Tao, X. (2022b). Electron dynamics in a chorus wave field generated from particle-in-cell simulations. *Geophysical Research Letters*, *49*(3), e2022GL097778. https://doi.org/10.1029/2022GL097778

Angelopoulos, V., Artemyev, A., Phan, T. D., & Miyashita, Y. (2020a). Near-Earth magnetotail reconnection powers space storms. *Nature Physics*, *16*(3), 317–321. https://doi.org/10.1038/s41567-019-0749-4

Angelopoulos, V., Cruce, P., Drozdov, A., Grimes, E. W., Hatzigeorgiu, N., King, D. A., et al. (2019). The space physics environment data analysis system (SPEDAS). *Space Science Reviews*, *215*(1), 9. https://doi.org/10.1007/s11214-018-0576-4

Angelopoulos, V., Tsai, E., Bingley, L., Shaffer, C., Turner, D. L., Runov, A., et al. (2020b). The ELFIN mission. *Space Science Reviews*, *216*(5), 103. https://doi.org/10.1007/s11214-020-00721-7

Angelopoulos, V., Zhang, X. J., Artemyev, A. V., Mourenas, D., Tsai, E., Wilkins, C., et al. (2023). Energetic electron precipitation driven by electromagnetic ion cyclotron waves from ELFIN's low altitude perspective. *Space Science Reviews*, *219*(37), 37. https://doi.org/10.1007/s11214-023-00984-w

Artemyev, A. V., Angelopoulos, V., Runov, A., & Petrukovich, A. A. (2016). Properties of current sheet thinning at x\sim 10 to 12 R_{E}. *Journal of Geophysical Research*, *121*(7), 6718–6731. https://doi.org/10.1002/2016JA022779

Artemyev, A. V., Demekhov, A. G., Zhang, X. J., Angelopoulos, V., Mourenas, D., Fedorenko, Y. V., et al. (2021). Role of ducting in relativistic electron loss by whistler-mode wave scattering. *Journal of Geophysical Research (Space Physics)*, *126*(11), e29851. https://doi.org/10.1029/2021JA029851

Artemyev, A. V., Mourenas, D., Zhang, X.-J., & Vainchtein, D. (2022). On the incorporation of nonlinear resonant wave-particle interactions into radiation belt models. *Journal of Geophysical Research*, *127*(9), e2022JA030853. https://doi.org/10.1029/2022JA030853

Aryan, H., Agapitov, O. V., Artemyev, A., Mourenas, D., Balikhin, M. A., Boynton, R., & Bortnik, J. (2020). Outer radiation belt electron lifetime model based on combined van allen probes and cluster VLF measurements. *Journal of Geophysical Research (Space Physics)*, *125*(8), e28018. https://doi.org/10.1029/2020JA028018

Birn, J., Hesse, M., & Schindler, K. (1996). MHD simulations of magnetotail dynamics. *Journal of Geophysical Research*, *101*(A6), 12939–12954. https://doi.org/10.1029/96JA00611

Birn, J., Runov, A., & Hesse, M. (2014). Energetic electrons in dipolarization events: Spatial properties and anisotropy. *Journal of Geophysical Research (Space Physics)*, *119*(5), 3604–3616. https://doi.org/10.1002/2013JA019738

Blake, J. B., Mauk, B. H., Baker, D. N., Carranza, P., Clemmons, J. H., Craft, J., et al. (2016). The fly's eye energetic particle spectrometer (FEEPS) sensors for the magnetospheric Multiscale (MMS) mission. *Space Science Reviews*, *199*(1–4), 309–329. https://doi.org/10.1007/s11214-015-0163-x

Blum, L. W., Li, X., & Denton, M. (2015). Rapid MeV electron precipitation as observed by SAMPEX/HILT during high-speed stream-driven storms. *Journal of Geophysical Research*, *120*(5), 3783–3794. https://doi.org/10.1002/2014JA020633

Boudouridis, A., Rodriguez, J. V., Kress, B. T., Dichter, B. K., & Onsager, T. G. (2020). Development of a bowtie inversion technique for real-time processing of the GOES-16/-17 SEISS MPS-HI electron channels. *Space Weather*, *18*(4), e02403. https://doi.org/10.1029/2019SW002403

Boynton, R. J., Mourenas, D., & Balikhin, M. A. (2016). Electron flux dropouts at Geostationary Earth Orbit: Occurrences, magnitudes, and main driving factors. *Journal of Geophysical Research (Space Physics)*, *121*(9), 8448–8461. https://doi.org/10.1002/2016JA022916

Boynton, R. J., Mourenas, D., & Balikhin, M. A. (2017). Electron flux dropouts at L\sim 4.2 from global positioning system satellites: Occurrences, magnitudes, and main driving factors. *Journal of Geophysical Research (Space Physics)*, *122*, 11. https://doi.org/10.1002/2017JA024523

Burch, J. L., Moore, T. E., Torbert, R. B., & Giles, B. L. (2016). Magnetospheric Multiscale overview and science objectives. *Space Science Reviews*, *199*(1–4), 5–21. https://doi.org/10.1007/s11214-015-0164-9

Capannolo, L., Li, W., Ma, Q., Qin, M., Shen, X. C., Angelopoulos, V., et al. (2023). Electron precipitation observed by ELFIN using proton precipitation as a proxy for electromagnetic ion cyclotron (EMIC) waves. *Geophysical Research Letters*, *50*(21), e2023GL103519. https://doi.org/10.1029/2023GL103519

Capannolo, L., Li, W., Ma, Q., Shen, X. C., Zhang, X. J., Redmon, R. J., et al. (2019). Energetic electron precipitation: Multievent analysis of its spatial extent during EMIC wave activity. *Journal of Geophysical Research (Space Physics)*, *124*(4), 2466–2483. https://doi.org/10.1029/2018JA026291

Carson, B. R., Rodger, C. J., & Clilverd, M. A. (2013). POES satellite observations of EMIC-wave driven relativistic electron precipitation during 1998–2010. *Journal of Geophysical Research*, *118*(1), 232–243. https://doi.org/10.1029/2012JA017998

Chen, H., Gao, X., Lu, Q., Tsurutani, B. T., & Wang, S. (2020). Statistical evidence for EMIC wave excitation driven by substorm injection and enhanced solar wind pressure in the Earth's magnetosphere: Two different EMIC wave sources. *Geophysical Research Letters*, *47*(21), e2020GL090275. https://doi.org/10.1029/2020GL090275

Chen, L., Thorne, R. M., Jordanova, V. K., Wang, C.-P., Gkioulidou, M., Lyons, L., & Horne, R. B. (2010). Global simulation of EMIC wave excitation during the 21 April 2001 storm from coupled RCM-RAM-HOTRAY modeling. *Journal of Geophysical Research (Space Physics)*, *115*(A7), A07209. https://doi.org/10.1029/2009JA015075

Cornwall, J. M., Coroniti, F. V., & Thorne, R. M. (1970). Turbulent loss of ring current protons. *Journal of Geophysical Research*, *75*(25), 4699–4709. https://doi.org/10.1029/JA075i025p04699

Denton, R. E., Ofman, L., Shprits, Y. Y., Bortnik, J., Millan, R. M., Rodger, C. J., et al. (2019). Pitch angle scattering of sub-MeV relativistic electrons by electromagnetic ion cyclotron waves. *Journal of Geophysical Research (Space Physics)*, *124*(7), 5610–5626. https://doi.org/10.1029/2018JA026384

Dichter, B. K., Galica, G. E., McGarity, J. O., Tsui, S., Golightly, M. J., Lopate, C., & Connell, J. J. (2015). Specification, design, and calibration of the space weather suite of instruments on the NOAA GOES-R Program spacecraft. *IEEE Transactions on Nuclear Science*, *62*(6), 2776–2783. https://doi.org/10.1109/TNS.2015.2477997

Drozdov, A. Y., Allison, H. J., Shprits, Y. Y., Usanova, M. E., Saikin, A., & Wang, D. (2022). Depletions of multi-MeV electrons and their association to minima in phase space density. *Geophysical Research Letters*, *49*(8), e2021GL097620. https://doi.org/10.1029/2021GL097620

Drozdov, A. Y., Shprits, Y. Y., Usanova, M. E., Aseev, N. A., Kellerman, A. C., & Zhu, H. (2017). EMIC wave parameterization in the long-term VERB code simulation. *Journal of Geophysical Research*, *122*(8), 8488–8501. https://doi.org/10.1002/2017JA024389

Drozdov, A. Y., Usanova, M. E., Hudson, M. K., Allison, H. J., & Shprits, Y. Y. (2020). The role of hiss, chorus, and EMIC waves in the modeling of the dynamics of the multi-MeV radiation belt electrons. *Journal of Geophysical Research*, *125*(9), e2020JA028282. https://doi.org/10.1029/2020JA028282

Dubyagin, S., Sergeev, V. A., & Kubyshkina, M. V. (2002). On the remote sensing of plasma sheet from low-altitude spacecraft. *Journal of Atmospheric and Solar-Terrestrial Physics*, *64*(5–6), 567–572. https://doi.org/10.1016/S1364-6826(02)00014-7

Evans, D. S., & Greer, M. S. (2004). Polar orbiting environmental satellite space environment monitor-2: Instrument description and archive data documentation.

Fu, X., Cowee, M. M., Friedel, R. H., Funsten, H. O., Gary, S. P., Hospodarsky, G. B., et al. (2014). Whistler anisotropy instabilities as the source of banded chorus: Van Allen Probes observations and particle-in-cell simulations. *Journal of Geophysical Research (Space Physics)*, *119*(10), 8288–8298. https://doi.org/10.1002/2014JA020364

Gabrielse, C., Angelopoulos, V., Runov, A., & Turner, D. L. (2014). Statistical characteristics of particle injections throughout the equatorial magnetotail. *Journal of Geophysical Research*, *119*(4), 2512–2535. https://doi.org/10.1002/2013JA019638

Gan, L., Li, W., Ma, Q., Artemyev, A. V., & Albert, J. M. (2022). Dependence of nonlinear effects on whistler-mode wave bandwidth and amplitude: A perspective from diffusion coefficients. *Journal of Geophysical Research*, *127*(5), e2021JA030063. https://doi.org/10.1029/2021JA030063

Gao, X., Li, W., Bortnik, J., Thorne, R. M., Lu, Q., Ma, Q., et al. (2015). The effect of different solar wind parameters upon significant relativistic electron flux dropouts in the magnetosphere. *Journal of Geophysical Research*, *120*(6), 4324–4337. https://doi.org/10.1002/2015JA021182

Glauert, S. A., & Horne, R. B. (2005). Calculation of pitch angle and energy diffusion coefficients with the PADIE code. *Journal of Geophysical Research*, *110*(A4), 4206. https://doi.org/10.1029/2004JA010851

Grach, V. S., Artemyev, A. V., Demekhov, A. G., Zhang, X.-J., Bortnik, J., Angelopoulos, V., et al. (2022a). Relativistic electron precipitation by emic waves: Importance of nonlinear resonant effects. *Geophysical Research Letters*, *49*(17), e2022GL099994. https://doi.org/10.1029/2022GL099994

Grach, V. S., Artemyev, A. V., Demekhov, A. G., Zhang, X.-J., Bortnik, J., Angelopoulos, V., et al. (2022b). Relativistic electron precipitation by EMIC waves: Importance of nonlinear resonant effects. *Geophysical Research Letters*, *49*(17), e99994. https://doi.org/10.1029/2022GL099994

Hendry, A. T., Rodger, C. J., & Clilverd, M. A. (2017). Evidence of sub-MeV EMIC-driven electron precipitation. *Geophysical Research Letters*, *44*(3), 1210–1218. https://doi.org/10.1002/2016GL071807

Hendry, A. T., Santolik, O., Kletzing, C. A., Rodger, C. J., Shiokawa, K., & Baishev, D. (2019). Multi-instrument observation of nonlinear EMIC-driven electron precipitation at sub-MeV energies. *Geophysical Research Letters*, *46*(13), 7248–7257. https://doi.org/10.1029/2019GL082401

Horne, R. B., & Thorne, R. M. (1993). On the preferred source location for the convective amplification of ion cyclotron waves. *Journal of Geophysical Research*, *98*(A6), 9233–9247. https://doi.org/10.1029/92JA02972

Horne, R. B., Thorne, R. M., Glauert, S. A., Albert, J. M., Meredith, N. P., & Anderson, R. R. (2005). Timescale for radiation belt electron acceleration by whistler mode chorus waves. *Journal of Geophysical Research*, *110*(A3), 3225. https://doi.org/10.1029/2004JA010811

Hua, M., Bortnik, J., & Ma, Q. (2022). Upper limit of outer radiation belt electron acceleration driven by whistler-mode chorus waves. *Geophysical Research Letters*, *49*(15), e2022GL099618. https://doi.org/10.1029/2022GL099618

Jaynes, A. N., Baker, D. N., Singer, H. J., Rodriguez, J. V., Loto'aniu, T. M., Ali, A. F., et al. (2015). Source and seed populations for relativistic electrons: Their roles in radiation belt changes. *Journal of Geophysical Research (Space Physics)*, *120*(9), 7240–7254. https://doi.org/10.1002/2015JA021234

Jun, C.-W., Miyoshi, Y., Kurita, S., Yue, C., Bortnik, J., Lyons, L., et al. (2021). The characteristics of EMIC waves in the magnetosphere based on the van allen probes and arase observations. *Journal of Geophysical Research (Space Physics)*, *126*(6), e29001. https://doi.org/10.1029/2020JA029001

Jun, C. W., Yue, C., Bortnik, J., Lyons, L. R., Nishimura, Y., & Kletzing, C. (2019). EMIC wave properties associated with and without injections in the inner magnetosphere. *Journal of Geophysical Research (Space Physics)*, *124*(3), 2029–2045. https://doi.org/10.1029/2018JA026279

Kasahara, S., Yokota, S., Hori, T., Keika, K., Miyoshi, Y., & Shinohara, I. (2018a). The mep-e instrument level-2 omni-directional flux data of exploration of energization and radiation in geospace (erg) arase satellite. *ERG Science Center, Institute for Space-Earth Environmental Research, Nagoya University*. https://doi.org/10.34515/DATA.ERG-02001

Kasahara, S., Yokota, S., Mitani, T., Asamura, K., Hirahara, M., Shibano, Y., & Takashima, T. (2018b). Medium-energy particle experiments-electron analyzer (MEP-e) for the exploration of energization and radiation in geospace (ERG) mission. *Earth Planets and Space*, *70*(1), 69. https://doi.org/10.1186/s40623-018-0847-z

Kasahara, Y., Kasaba, Y., Kojima, H., Yagitani, S., Ishisaka, K., Kumamoto, A., et al. (2018c). The plasma wave experiment (PWE) on board the arase (ERG) satellite. *Earth Planets and Space*, *70*(1), 86. https://doi.org/10.1186/s40623-018-0842-4

Kasahara, Y., Kojima, H., Matsuda, S., Ozaki, S., Yagitani, M., Shoji, M., et al. (2018d). The pwe/ofa instrument level-2 power spectrum data of exploration of energization and radiation in geospace (erg) arase satellite. *ERG Science Center, Institute for Space-Earth Environmental Research, Nagoya*. https://doi.org/10.34515/DATA.ERG-08000

Kennel, C. F. (1969). Consequences of a magnetospheric plasma. *Reviews of Geophysics and Space Physics*, *7*(1–2), 379–419. https://doi.org/10.1029/RG007i001p00379

Kennel, C. F., & Petschek, H. E. (1966). Limit on stably trapped particle fluxes. *Journal of Geophysical Research*, *71*, 1–28. https://doi.org/10.1029/jz071i001p00001

Kersten, T., Horne, R. B., Glauert, S. A., Meredith, N. P., Fraser, B. J., & Grew, R. S. (2014). Electron losses from the radiation belts caused by EMIC waves. *Journal of Geophysical Research*, *119*(11), 8820–8837. https://doi.org/10.1002/2014JA020366

Kim, H., Schiller, Q., Engebretson, M. J., Noh, S., Kuzichev, I., Lanzerotti, L. J., et al. (2021a). Observations of particle loss due to injection associated electromagnetic ion cyclotron waves. *Journal of Geophysical Research (Space Physics)*, *126*(2), e28503. https://doi.org/10.1029/2020JA028503

Kim, H.-J., & Chan, A. A. (1997). Fully adiabatic changes in storm time relativistic electron fluxes. *Journal of Geophysical Research*, *102*(A10), 22107–22116. https://doi.org/10.1029/97JA01814

Kim, H.-J., Lee, D.-Y., Wolf, R., Bortnik, J., Kim, K.-C., Lyons, L., et al. (2021b). Rapid injections of MeV electrons and extremely fast step-like outer radiation belt enhancements. *Geophysical Research Letters*, *48*(9), e2021GL093151. https://doi.org/10.1029/2021GL093151

Kozyra, J. U., Jordanova, V. K., Home, R. B., & Thorne, R. M. (1997). Modeling of the contribution of electromagnetic ion cyclotron (EMIC) waves to stormtime ring current erosion. *Washington DC American Geophysical Union Geophysical Monograph Series*, *98*, 187–202. https://doi.org/10.1029/GM098p0187

Kubota, Y., & Omura, Y. (2017). Rapid precipitation of radiation belt electrons induced by EMIC rising tone emissions localized in longitude inside and outside the plasmapause. *Journal of Geophysical Research (Space Physics)*, *122*(1), 293–309. https://doi.org/10.1002/2016JA023267

Kubota, Y., Omura, Y., & Summers, D. (2015). Relativistic electron precipitation induced by EMIC-triggered emissions in a dipole magnetosphere. *Journal of Geophysical Research (Space Physics)*, *120*(6), 4384–4399. https://doi.org/10.1002/2015JA021017

Kurita, S., Miyoshi, Y., Shiokawa, K., Higashio, N., Mitani, T., Takashima, T., et al. (2018). Rapid loss of relativistic electrons by EMIC waves in the outer radiation belt observed by arase, van allen probes, and the PWING ground stations. *Geophysical Research Letters*, *45*(23), 12720–12729. https://doi.org/10.1029/2018GL080262

Li, W., Ni, B., Thorne, R. M., Bortnik, J., Green, J. C., Kletzing, C. A., et al. (2013). Constructing the global distribution of chorus wave intensity using measurements of electrons by the POES satellites and waves by the Van Allen Probes. *Geophysical Research Letters*, *40*(17), 4526–4532. https://doi.org/10.1002/grl.50920

Li, W., Santolik, O., Bortnik, J., Thorne, R. M., Kletzing, C. A., Kurth, W. S., & Hospodarsky, G. B. (2016). New chorus wave properties near the equator from Van Allen Probes wave observations. *Geophysical Research Letters*, *43*(10), 4725–4735. https://doi.org/10.1002/2016GL068780

Li, W., Shprits, Y. Y., & Thorne, R. M. (2007). Dynamic evolution of energetic outer zone electrons due to wave-particle interactions during storms. *Journal of Geophysical Research*, *112*(A10), 10220. https://doi.org/10.1029/2007JA012368

Li, W., Thorne, R. M., Ma, Q., Ni, B., Bortnik, J., Baker, D. N., et al. (2014). Radiation belt electron acceleration by chorus waves during the 17 March 2013 storm. *Journal of Geophysical Research*, *119*(6), 4681–4693. https://doi.org/10.1002/2014JA019945

Li, W., Thorne, R. M., Nishimura, Y., Bortnik, J., Angelopoulos, V., McFadden, J. P., et al. (2010). THEMIS analysis of observed equatorial electron distributions responsible for the chorus excitation. *Journal of Geophysical Research*, *115*(A6), A00F11. https://doi.org/10.1029/2009JA014845

Ma, Q., Connor, H. K., Zhang, X. J., Li, W., Shen, X. C., Gillespie, D., et al. (2020). Global survey of plasma sheet electron precipitation due to whistler mode chorus waves in Earth's magnetosphere. *Geophysical Research Letters*, *47*(15), e88798. https://doi.org/10.1029/2020GL088798

Ma, Q., Li, W., Thorne, R. M., Ni, B., Kletzing, C. A., Kurth, W. S., et al. (2015). Modeling inward diffusion and slow decay of energetic electrons in the Earth's outer radiation belt. *Geophysical Research Letters*, *42*(4), 987–995. https://doi.org/10.1002/2014GL062977

Ma, Q., Mourenas, D., Artemyev, A., Li, W., Thorne, R. M., & Bortnik, J. (2016). Strong enhancement of 10-100 keV electron fluxes by combined effects of chorus waves and time domain structures. *Geophysical Research Letters*, *43*(10), 4683–4690. https://doi.org/10.1002/2016GL069125

Matsuda, S., Kasahara, Y., Kojima, H., Kasaba, Y., Yagitani, S., Ozaki, M., et al. (2018). Onboard software of plasma wave experiment aboard arase: Instrument management and signal processing of waveform capture/onboard frequency analyzer. *Earth Planets and Space*, *70*(1), 75. https://doi.org/10.1186/s40623-018-0838-0

Matsumura, C., Miyoshi, Y., Seki, K., Saito, S., Angelopoulos, V., & Koller, J. (2011). Outer radiation belt boundary location relative to the magnetopause: Implications for magnetopause shadowing. *Journal of Geophysical Research (Space Physics)*, *116*(A6), A06212. https://doi.org/10.1029/2011JA016575

Matsuoka, A., Teramoto, M., Imajo, S., Kurita, S., Miyoshi, Y., & Shinohara, I. (2018a). The mgf instrument level-2 high-resolution magnetic field data of exploration of energization and radiation in geospace (erg) arase satellite. *ERG Science Center, Institute for Space-Earth Environmental Research, Nagoya*. https://doi.org/10.34515/DATA.ERG-06000

Matsuoka, A., Teramoto, M., Nomura, R., Nosé, M., Fujimoto, A., Tanaka, Y., et al. (2018b). The ARASE (ERG) magnetic field investigation. *Earth Planets and Space*, *70*(1), 43. https://doi.org/10.1186/s40623-018-0800-1

Mauk, B. H., Blake, J. B., Baker, D. N., Clemmons, J. H., Reeves, G. D., Spence, H. E., et al. (2016). The energetic particle detector (EPD) investigation and the energetic ion spectrometer (EIS) for the magnetospheric Multiscale (MMS) mission. *Space Science Reviews*, *199*(1–4), 471–514. https://doi.org/10.1007/s11214-014-0055-5

Meredith, N. P., Cain, M., Horne, R. B., Thorne, R. M., Summers, D., & Anderson, R. R. (2003). Evidence for chorus-driven electron acceleration to relativistic energies from a survey of geomagnetically disturbed periods. *Journal of Geophysical Research*, *108*(A6), 1248. https://doi.org/10.1029/2002JA009764

Meredith, N. P., Horne, R. B., & Anderson, R. R. (2001). Substorm dependence of chorus amplitudes: Implications for the acceleration of electrons to relativistic energies. *Journal of Geophysical Research*, *106*(A7), 13165–13178. https://doi.org/10.1029/2000JA900156

Meredith, N. P., Horne, R. B., Kersten, T., Fraser, B. J., & Grew, R. S. (2014). Global morphology and spectral properties of EMIC waves derived from CRRES observations. *Journal of Geophysical Research*, *119*(7), 5328–5342. https://doi.org/10.1002/2014JA020064

Millan, R. M., & Thorne, R. M. (2007). Review of radiation belt relativistic electron losses. *Journal of Atmospheric and Solar-Terrestrial Physics*, *69*(3), 362–377. https://doi.org/10.1016/j.jastp.2006.06.019

Mitani, T., Hori, T., Park, I., Takashima, T., Miyoshi, Y., & Shinohara, I. (2018a). The hep instrument level-2 omni-directional flux data of exploration of energization and radiation in geospace (erg) arase satellite. *ERG Science Center, Institute for Space-Earth Environmental Research, Nagoya*. https://doi.org/10.34515/DATA.ERG-01001

Mitani, T., Takashima, T., Kasahara, S., Miyake, W., & Hirahara, M. (2018b). High-energy electron experiments (HEP) aboard the ERG (Arase) satellite. *Earth Planets and Space*, *70*(1), 77. https://doi.org/10.1186/s40623-018-0853-1

Miyoshi, Y., Hori, T., Shoji, M., Teramoto, M., Chang, T. F., Segawa, T., et al. (2018a). The ERG science center. *Earth Planets and Space*, *70*(1), 96. https://doi.org/10.1186/s40623-018-0867-8

Miyoshi, Y., Kataoka, R., Kasahara, Y., Kumamoto, A., Nagai, T., & Thomsen, M. F. (2013). High-speed solar wind with southward interplanetary magnetic field causes relativistic electron flux enhancement of the outer radiation belt via enhanced condition of whistler waves. *Geophysical Research Letters*, *40*(17), 4520–4525. https://doi.org/10.1002/grl.50916

Miyoshi, Y., Morioka, A., Misawa, H., Obara, T., Nagai, T., & Kasahara, Y. (2003). Rebuilding process of the outer radiation belt during the 3 November 1993 magnetic storm: NOAA and Exos-D observations. *Journal of Geophysical Research*, *108*(A1), 1004. https://doi.org/10.1029/2001JA007542

Miyoshi, Y., Sakaguchi, K., Shiokawa, K., Evans, D., Albert, J., Connors, M., & Jordanova, V. (2008). Precipitation of radiation belt electrons by EMIC waves, observed from ground and space. *Geophysical Research Letters*, *35*(23), L23101. https://doi.org/10.1029/2008GL035727

Miyoshi, Y., Shinohara, I., & Jun, C.-W. (2018b). The level-2 orbit data of exploration of energization and radiation in geospace (erg) arase satellite. *ERG Science Center, Institute for Space-Earth Environmental Research, Nagoya*. https://doi.org/10.34515/DATA.ERG-12000

Miyoshi, Y., Shinohara, I., Takashima, T., Asamura, K., Higashio, N., Mitani, T., et al. (2018c). Geospace exploration project ERG. *Earth Planets and Space*, *70*(1), 101. https://doi.org/10.1186/s40623-018-0862-0

Mourenas, D., Artemyev, A., Agapitov, O., & Krasnoselskikh, V. (2012). Acceleration of radiation belts electrons by oblique chorus waves. *Journal of Geophysical Research*, *117*(A10), 10212. https://doi.org/10.1029/2012JA018041

Mourenas, D., Artemyev, A. V., Agapitov, O. V., & Krasnoselskikh, V. (2014a). Consequences of geomagnetic activity on energization and loss of radiation belt electrons by oblique chorus waves. *Journal of Geophysical Research*, *119*(4), 2775–2796. https://doi.org/10.1002/2013JA019674

Mourenas, D., Artemyev, A. V., Agapitov, O. V., Krasnoselskikh, V., & Li, W. (2014b). Approximate analytical solutions for the trapped electron distribution due to quasi-linear diffusion by whistler mode waves. *Journal of Geophysical Research*, *119*(12), 9962–9977. https://doi.org/10.1002/2014JA020443

Mourenas, D., Artemyev, A. V., Ma, Q., Agapitov, O. V., & Li, W. (2016). Fast dropouts of multi-MeV electrons due to combined effects of EMIC and whistler mode waves. *Geophysical Research Letters*, *43*(9), 4155–4163. https://doi.org/10.1002/2016GL068921

Mourenas, D., Artemyev, A. V., Zhang, X.-J., & Angelopoulos, V. (2022a). Extreme energy spectra of relativistic electron flux in the outer radiation belt. *Journal of Geophysical Research: Space Physics*, *127*(11), e2022JA031038. https://doi.org/10.1029/2022JA031038

Mourenas, D., Artemyev, A. V., Zhang, X. J., & Angelopoulos, V. (2022b). Extreme energy spectra of relativistic electron flux in the outer radiation belt. *Journal of Geophysical Research (Space Physics)*, *127*(11), e2022JA031038. https://doi.org/10.1029/2022JA031038

Mourenas, D., Artemyev, A. V., Zhang, X. J., & Angelopoulos, V. (2023). Upper limit on outer radiation belt electron flux based on dynamical equilibrium. *Journal of Geophysical Research (Space Physics)*, *128*(8), e2023JA031676. https://doi.org/10.1029/2023JA031676

Mourenas, D., Artemyev, A. V., Zhang, X.-J., & Angelopoulos, V. (2024). Impact of EMIC waves on electron flux dropouts measured by GPS spacecraft: Insights from ELFIN. *Journal of Geophysical Research: Space Physics*, *129*(10), e2024JA032984. https://doi.org/10.1029/2024JA032984

Mourenas, D., Artemyev, A. V., Zhang, X.-J., Angelopoulos, V., Tsai, E., & Wilkins, C. (2021). Electron lifetimes and diffusion rates inferred from ELFIN measurements at low altitude: First results. *Journal of Geophysical Research: Space Physics*, *126*(11), e2021JA029757. https://doi.org/10.1029/2021JA029757

Mourenas, D., Zhang, X. J., Nunn, D., Artemyev, A. V., Angelopoulos, V., Tsai, E., & Wilkins, C. (2022). Short chorus wave packets: Generation within chorus elements, statistics, and consequences on energetic electron precipitation. *Journal of Geophysical Research (Space Physics)*, *127*(5), e30310. https://doi.org/10.1029/2022JA030310

Nakamura, S., Miyoshi, Y., Shiokawa, K., Omura, Y., Mitani, T., Takashima, T., et al. (2022). Simultaneous observations of EMIC-induced drifting electron holes (EDEHs) in the Earth's radiation belt by the arase satellite, Van Allen probes, and THEMIS. *Geophysical Research Letters*, *49*(5), e2021GL095194. https://doi.org/10.1029/2021GL095194

Ni, B., Cao, X., Zou, Z., Zhou, C., Gu, X., Bortnik, J., et al. (2015). Resonant scattering of outer zone relativistic electrons by multiband EMIC waves and resultant electron loss time scales. *Journal of Geophysical Research*, *120*(9), 7357–7373. https://doi.org/10.1002/2015JA021466

Olifer, L., Mann, I. R., Boyd, A. J., Ozeke, L. G., & Choi, D. (2018). On the role of Last closed drift shell dynamics in driving fast losses and van allen radiation belt extinction. *Journal of Geophysical Research*, *123*, 3692–3703. https://doi.org/10.1029/2018JA025190

Olson, J. C., & Lee, L. V. (1983). Pc1 wave generation by sudden impulses. *Planetary and Space Science*, *31*(3), 295–302. https://doi.org/10.1016/0032-0633(83)90079-X

Omura, Y., Furuya, N., & Summers, D. (2007). Relativistic turning acceleration of resonant electrons by coherent whistler mode waves in a dipole magnetic field. *Journal of Geophysical Research*, *112*(A6), 6236. https://doi.org/10.1029/2006JA012243

Omura, Y., Katoh, Y., & Summers, D. (2008). Theory and simulation of the generation of whistler-mode chorus. *Journal of Geophysical Research*, *113*(A4), 4223. https://doi.org/10.1029/2007JA012622

Ozeke, L. G., Mann, I. R., Dufresne, S., Olifer, L., Morley, S., Claudepierre, S., et al. (2020). Rapid outer radiation belt flux dropouts and fast acceleration during the March 2015 and 2013 storms: The role of ULF wave transport from a dynamic outer boundary. *Journal of Geophysical Research*, *125*(2), e2019JA027179. https://doi.org/10.1029/2019JA027179

Ozeke, L. G., Mann, I. R., Murphy, K. R., Jonathan Rae, I., & Milling, D. K. (2014). Analytic expressions for ULF wave radiation belt radial diffusion coefficients. *Journal of Geophysical Research*, *119*(3), 1587–1605. https://doi.org/10.1002/2013JA019204

Pinto, V. A., Zhang, X.-J., Mourenas, D., Bortnik, J., Artemyev, A. V., Lyons, L. R., & Moya, P. S. (2020). On the confinement of ultrarelativistic electron remnant belts to low L shells. *Journal of Geophysical Research*, *125*(3), e27469. https://doi.org/10.1029/2019JA027469

Ross, J. P. J., Glauert, S. A., Horne, R. B., Watt, C. E. J., & Meredith, N. P. (2021). On the variability of emic waves and the consequences for the relativistic electron radiation belt population. *Journal of Geophysical Research: Space Physics*, *126*(12), e2975426. https://doi.org/10.1029/2021JA029754

Ross, J. P. J., Meredith, N. P., Glauert, S. A., Horne, R. B., & Clilverd, M. A. (2019). Effects of VLF transmitter waves on the inner belt and slot region. *Journal of Geophysical Research (Space Physics)*, *124*(7), 5260–5277. https://doi.org/10.1029/2019JA026716

Runov, A., Angelopoulos, V., Gabrielse, C., Liu, J., Turner, D. L., & Zhou, X.-Z. (2015). Average thermodynamic and spectral properties of plasma in and around dipolarizing flux bundles. *Journal of Geophysical Research*, *120*(6), 4369–4383. https://doi.org/10.1002/2015JA021166

Russell, C. T., Anderson, B. J., Baumjohann, W., Bromund, K. R., Dearborn, D., Fischer, D., et al. (2016). The magnetospheric Multiscale magnetometers. *Space Science Reviews*, *199*(1–4), 189–256. https://doi.org/10.1007/s11214-014-0057-3

Sandanger, M., Søraas, F., Aarsnes, K., Oksavik, K., & Evans, D. S. (2007). Loss of relativistic electrons: Evidence for pitch angle scattering by electromagnetic ion cyclotron waves excited by unstable ring current protons. *Journal of Geophysical Research*, *112*(A12), A12213. https://doi.org/10.1029/2006JA012138

Santolík, O., Kletzing, C. A., Kurth, W. S., Hospodarsky, G. B., & Bounds, S. R. (2014). Fine structure of large-amplitude chorus wave packets. *Geophysical Research Letters*, *41*(2), 293–299. https://doi.org/10.1002/2013GL058889

SantolíK, O., Gurnett, D. A., Pickett, J. S., Parrot, M., & Cornilleau-Wehrlin, N. (2003). Spatio-temporal structure of storm-time chorus. *Journal of Geophysical Research*, *108*(A7), 1278. https://doi.org/10.1029/2002JA009791

Schulz, M., & Lanzerotti, L. J. (1974). *Particle diffusion in the radiation belts*. Springer.

Sergeev, V. A., Angelopoulos, V., Kubyshkina, M., Donovan, E., Zhou, X.-Z., Runov, A., et al. (2011). Substorm growth and expansion onset as observed with ideal ground-spacecraft THEMIS coverage. *Journal of Geophysical Research*, *116*(A5), A00I26. https://doi.org/10.1029/2010JA015689

Shane, A. D., Marshall, R. A., Claudepierre, S. G., & Pettit, J. M. (2023). Electron lifetimes measured at LEO: Comparison with RBSP estimates and pitch angle resolved lifetimes. *Journal of Geophysical Research*, *128*(8), e2023JA031679. https://doi.org/10.1029/2023JA031679

Sheeley, B. W., Moldwin, M. B., Rassoul, H. K., & Anderson, R. R. (2001). An empirical plasmasphere and trough density model: CRRES observations. *Journal of Geophysical Research*, *106*(A11), 25631–25642. https://doi.org/10.1029/2000JA000286

Shi, R., Summers, D., Ni, B., Fennell, J. F., Blake, J. B., Spence, H. E., & Reeves, G. D. (2016). Survey of radiation belt energetic electron pitch angle distributions based on the Van Allen Probes MagEIS measurements. *Journal of Geophysical Research (Space Physics)*, *121*(2), 1078–1090. https://doi.org/10.1002/2015JA021724

Shi, X., Zhang, X.-J., Artemyev, A., Angelopoulos, V., Hartinger, M. D., Tsai, E., & Wilkins, C. (2022). On the role of ULF waves in the spatial and temporal periodicity of energetic electron precipitation. *Journal of Geophysical Research (Space Physics)*, *127*(12), e2022JA030932. https://doi.org/10.1029/2022JA030932

Shprits, Y. Y., Chen, L., & Thorne, R. M. (2009). Simulations of pitch angle scattering of relativistic electrons with MLT-dependent diffusion coefficients. *Journal of Geophysical Research*, *114*(A3), A03219. https://doi.org/10.1029/2008JA013695

Shprits, Y. Y., Drozdov, A. Y., Spasojevic, M., Kellerman, A. C., Usanova, M. E., Engebretson, M. J., et al. (2016). Wave-induced loss of ultra-relativistic electrons in the Van Allen radiation belts. *Nature Communications*, *7*(1), 12883. https://doi.org/10.1038/ncomms12883

Shprits, Y. Y., Kellerman, A., Aseev, N., Drozdov, A. Y., & Michaelis, I. (2017). Multi-MeV electron loss in the heart of the radiation belts. *Geophysical Research Letters*, *44*(3), 1204–1209. https://doi.org/10.1002/2016GL072258

Shprits, Y. Y., Subbotin, D. A., Meredith, N. P., & Elkington, S. R. (2008). Review of modeling of losses and sources of relativistic electrons in the outer radiation belt II: Local acceleration and loss. *Journal of Atmospheric and Solar-Terrestrial Physics*, *70*(14), 1694–1713. https://doi.org/10.1016/j.jastp.2008.06.014

Shprits, Y. Y., Thorne, R. M., Friedel, R., Reeves, G. D., Fennell, J., Baker, D. N., & Kanekal, S. G. (2006a). Outward radial diffusion driven by losses at magnetopause. *Journal of Geophysical Research*, *111*(A11), 11214. https://doi.org/10.1029/2006JA011657

Shprits, Y. Y., Thorne, R. M., Horne, R. B., & Summers, D. (2006b). Bounce-averaged diffusion coefficients for field-aligned chorus waves. *Journal of Geophysical Research*, *111*(A10), 10225. https://doi.org/10.1029/2006JA011725

Shue, J.-H., Chao, J. K., Fu, H. C., Russell, C. T., Song, P., Khurana, K. K., & Singer, H. J. (1997). A new functional form to study the solar wind control of the magnetopause size and shape. *Journal of Geophysical Research*, *102*(A5), 9497–9512. https://doi.org/10.1029/97JA00196

Singer, H. J., Matheson, L., Grubb, R., Newman, A., & Bouwer, S. D. (1996). Monitoring space weather with the goes magnetometers in goes-8 and beyond. In E. washwell (Ed.), *SPIE conference proceedings*. (Tech. Rep. No. 2812.

Sorathia, K. A., Ukhorskiy, A. Y., Merkin, V. G., Fennell, J. F., & Claudepierre, S. G. (2018). Modeling the depletion and recovery of the outer radiation belt during a geomagnetic storm: Combined MHD and test particle simulations. *Journal of Geophysical Research (Space Physics)*, *123*(7), 5590–5609. https://doi.org/10.1029/2018JA025506

Su, Z., Zhu, H., Xiao, F., Zheng, H., Shen, C., Wang, Y., & Wang, S. (2012). Bounce-averaged advection and diffusion coefficients for monochromatic electromagnetic ion cyclotron wave: Comparison between test-particle and quasi-linear models. *Journal of Geophysical Research (Space Physics)*, *117*(A9), A09222. https://doi.org/10.1029/2012JA017917

Summers, D., Ni, B., & Meredith, N. P. (2007a). Timescales for radiation belt electron acceleration and loss due to resonant wave-particle interactions: 1. Theory. *Journal of Geophysical Research*, *112*(A4), 4206. https://doi.org/10.1029/2006JA011801

Summers, D., Ni, B., & Meredith, N. P. (2007b). Timescales for radiation belt electron acceleration and loss due to resonant wave-particle interactions: 2. Evaluation for VLF chorus, ELF hiss, and electromagnetic ion cyclotron waves. *Journal of Geophysical Research*, *112*(A4), 4207. https://doi.org/10.1029/2006JA011993

Summers, D., & Stone, S. (2022). Analysis of radiation belt killer electron energy spectra. *Journal of Geophysical Research*, *127*(9), e2022JA030698. https://doi.org/10.1029/2022JA030698

Summers, D., & Thorne, R. M. (2003). Relativistic electron pitch-angle scattering by electromagnetic ion cyclotron waves during geomagnetic storms. *Journal of Geophysical Research*, *108*(A4), 1143. https://doi.org/10.1029/2002JA009489

Summers, D., Thorne, R. M., & Xiao, F. (1998). Relativistic theory of wave-particle resonant diffusion with application to electron acceleration in the magnetosphere. *Journal of Geophysical Research*, *103*(A9), 20487–20500. https://doi.org/10.1029/98JA01740

Tang, C. L., Wang, X., Ni, B. B., Su, Z. P., & Zhang, J. C. (2022). The 600 keV electron injections in the Earth's outer radiation belt: A statistical study. *Earth and Planetary Physics*, *6*(2), 149–160. https://doi.org/10.26464/epp2022012

Tao, X., Thorne, R. M., Li, W., Ni, B., Meredith, N. P., & Horne, R. B. (2011). Evolution of electron pitch angle distributions following injection from the plasma sheet. *Journal of Geophysical Research*, *116*(A4), A04229. https://doi.org/10.1029/2010JA016245

Thorne, R. M., & Kennel, C. F. (1971). Relativistic electron precipitation during magnetic storm main phase. *Journal of Geophysical Research*, *76*(19), 4446–4453. https://doi.org/10.1029/JA076i019p04446

Thorne, R. M., Li, W., Ni, B., Ma, Q., Bortnik, J., Chen, L., et al. (2013). Rapid local acceleration of relativistic radiation-belt electrons by magnetospheric chorus. *Nature*, *504*(7480), 411–414. https://doi.org/10.1038/nature12889

Tsai, E., Artemyev, A., Zhang, X.-J., & Angelopoulos, V. (2022). Relativistic electron precipitation driven by nonlinear resonance with whistler-mode waves. *Journal of Geophysical Research (Space Physics)*, *127*(5), e30338. https://doi.org/10.1029/2022JA030338

Tsurutani, B. T., & Smith, E. J. (1974). Postmidnight chorus: A substorm phenomenon. *Journal of Geophysical Research*, *79*(1), 118–127. https://doi.org/10.1029/JA079i001p00118

Tsyganenko, N. A. (1989). A magnetospheric magnetic field model with a warped tail current sheet. *Planetary and Space Science*, *37*(1), 5–20. https://doi.org/10.1016/0032-0633(89)90066-4

Tsyganenko, N. A. (2002a). A model of the near magnetosphere with a dawn-dusk asymmetry 1. Mathematical structure. *Journal of Geophysical Research*, *107*(A8), 15. https://doi.org/10.1029/2001JA000219

Tsyganenko, N. A. (2002b). A model of the near magnetosphere with a dawn-dusk asymmetry 2. Parameterization and fitting to observations. *Journal of Geophysical Research*, *107*(A8), 17. https://doi.org/10.1029/2001JA000220

Tsyganenko, N. A., & Sitnov, M. I. (2005). Modeling the dynamics of the inner magnetosphere during strong geomagnetic storms. *Journal of Geophysical Research*, *110*(A3), A03208. https://doi.org/10.1029/2004JA010798

Turner, D. L., Angelopoulos, V., Li, W., Bortnik, J., Ni, B., Ma, Q., et al. (2014). Competing source and loss mechanisms due to wave-particle interactions in Earth's outer radiation belt during the 30 September to 3 October 2012 geomagnetic storm. *Journal of Geophysical Research*, *119*, 1960–1979. https://doi.org/10.1002/2014JA019770

Turner, D. L., Angelopoulos, V., Shprits, Y., Kellerman, A., Cruce, P., & Larson, D. (2012a). Radial distributions of equatorial phase space density for outer radiation belt electrons. *Geophysical Research Letters*, *39*(9), L09101. https://doi.org/10.1029/2012GL051722

Turner, D. L., Shprits, Y., Hartinger, M., & Angelopoulos, V. (2012b). Explaining sudden losses of outer radiation belt electrons during geomagnetic storms. *Nature Physics*, *8*(3), 208–212. https://doi.org/10.1038/nphys2185

Ukhorskiy, A. Y., Sitnov, M. I., Millan, R. M., & Kress, B. T. (2011). The role of drift orbit bifurcations in energization and loss of electrons in the outer radiation belt. *Journal of Geophysical Research*, *116*(A9), 9208. https://doi.org/10.1029/2011JA016623

Ukhorskiy, A. Y., Sorathia, K. A., Merkin, V. G., Crabtree, C., Fletcher, A. C., Malaspina, D. M., & Schwartz, S. J. (2022). Cross-scale energy cascade powered by magnetospheric convection. *Scientific Reports*, *12*(1), 4446. https://doi.org/10.1038/s41598-022-08038-x

Usanova, M. E., Drozdov, A., Orlova, K., Mann, I. R., Shprits, Y., Robertson, M. T., et al. (2014). Effect of EMIC waves on relativistic and ultrarelativistic electron populations: Ground-based and Van Allen Probes observations. *Geophysical Research Letters*, *41*(5), 1375–1381. https://doi.org/10.1002/2013GL059024

Usanova, M. E., Mann, I. R., Kale, Z. C., Rae, I. J., Sydora, R. D., Sandanger, M., et al. (2010). Conjugate ground and multisatellite observations of compression-related EMIC Pc1 waves and associated proton precipitation. *Journal of Geophysical Research (Space Physics)*, *115*(A7), A07208. https://doi.org/10.1029/2009JA014935

Walt, M. (1994). Introduction to geomagnetically trapped radiation. *Camb. Atmos. Space Sci. Ser.*, *10*, 10.

Wilkins, C., Angelopoulos, V., Runov, A., Artemyev, A., Zhang, X. J., Liu, J., & Tsai, E. (2023). Statistical characteristics of the electron isotropy boundary. *Journal of Geophysical Research (Space Physics)*, *128*(10), e2023JA031774. https://doi.org/10.1029/2023JA031774

Yahnin, A., & Yahnina, T. (2007). Energetic proton precipitation related to ion cyclotron waves. *Journal of Atmospheric and Solar-Terrestrial Physics*, *69*(14), 1690–1706. https://doi.org/10.1016/j.jastp.2007.02.010

Yahnin, A. G., Yahnina, T. A., Raita, T., & Manninen, J. (2017). Ground pulsation magnetometer observations conjugated with relativistic electron precipitation. *Journal of Geophysical Research (Space Physics)*, *122*(9), 9169–9182. https://doi.org/10.1002/2017JA024249

Yahnin, A. G., Yahnina, T. A., Semenova, N. V., Gvozdevsky, B. B., & Pashin, A. B. (2016). Relativistic electron precipitation as seen by NOAA POES. *Journal of Geophysical Research (Space Physics)*, *121*(9), 8286–8299. https://doi.org/10.1002/2016JA022765

Yokota, S., Kasahara, S., Mitani, T., Asamura, K., Hirahara, M., Takashima, T., et al. (2017). Medium-energy particle experiments-ion mass analyzer (MEP-i) onboard ERG (Arase). *Earth Planets and Space*, *69*(1), 172. https://doi.org/10.1186/s40623-017-0754-8

Yu, Y., Koller, J., Zaharia, S., & Jordanova, V. (2012). L{\midast} neural networks from different magnetic field models and their applicability. *Space Weather*, *10*(2), S02014. https://doi.org/10.1029/2011SW000743

Zhang, X., Angelopoulos, V., Artemyev, A. V., & Liu, J. (2018). Whistler and electron firehose instability control of electron distributions in and around dipolarizing flux bundles. *Geophysical Research Letters*, *45*(18), 9380–9389. https://doi.org/10.1029/2018GL079613

Zhang, X. J., Agapitov, O., Artemyev, A. V., Mourenas, D., Angelopoulos, V., Kurth, W. S., et al. (2020a). Phase decoherence within intense chorus wave packets constrains the efficiency of nonlinear resonant electron acceleration. *Geophysical Research Letters*, *47*(20), e89807. https://doi.org/10.1029/2020GL089807

Zhang, X.-J., Angelopoulos, V., Artemyev, A., Mourenas, D., Agapitov, O., Tsai, E., & Wilkins, C. (2023). Temporal scales of electron precipitation driven by whistler-mode waves. *Journal of Geophysical Research (Space Physics)*, *128*(1), e2022JA031087. https://doi.org/10.1029/2022JA031087

Zhang, X.-J., Li, W., Thorne, R. M., Angelopoulos, V., Bortnik, J., Kletzing, C. A., et al. (2016). Statistical distribution of EMIC wave spectra: Observations from van allen probes. *Geophysical Research Letters*, *43*(24), 12. https://doi.org/10.1002/2016GL071158

Zhang, X. J., Mourenas, D., Artemyev, A. V., Angelopoulos, V., Bortnik, J., Thorne, R. M., et al. (2019). Nonlinear electron interaction with intense chorus waves: Statistics of occurrence rates. *Geophysical Research Letters*, *46*(13), 7182–7190. https://doi.org/10.1029/2019GL083833

Zhang, X. J., Mourenas, D., Artemyev, A. V., Angelopoulos, V., Kurth, W. S., Kletzing, C. A., & Hospodarsky, G. B. (2020b). Rapid frequency variations within intense chorus wave packets. *Geophysical Research Letters*, *47*(15), e88853. https://doi.org/10.1029/2020GL088853

Zhang, X.-J., Mourenas, D., Artemyev, A. V., Angelopoulos, V., & Thorne, R. M. (2017). Contemporaneous EMIC and whistler mode waves: Observations and consequences for MeV electron loss. *Geophysical Research Letters*, *44*(16), 8113–8121. https://doi.org/10.1002/2017GL073886

Zhang, X. J., Mourenas, D., Shen, X. C., Qin, M., Artemyev, A. V., Ma, Q., et al. (2021). Dependence of relativistic electron precipitation in the ionosphere on EMIC wave minimum resonant energy at the conjugate equator. *Journal of Geophysical Research (Space Physics)*, *126*(5), e29193. https://doi.org/10.1029/2021JA029193